Single-cell transcriptomic analysis of the lateral hypothalamic area reveals molecularly distinct populations of inhibitory and excitatory neurons

Laura E. Mickelsen[1,2,8], **Mohan Bolisetty**[3,7,8], **Brock R. Chimileski**[1], **Akie Fujita**[1,2,4], **Eric J. Beltrami**[1], **James T. Costanzo**[1], **Jacob R. Naparstek**[1], **Paul Robson**[3,5,6,*], **Alexander C. Jackson**[1,2,6,*]

[1]Department of Physiology and Neurobiology, University of Connecticut, Storrs, CT, USA.

[2]Connecticut Institute for the Brain and Cognitive Sciences, Storrs, CT, USA.

[3]The Jackson Laboratory for Genomic Medicine, Farmington, CT, USA.

[4]Department of Biomedical Engineering, University of Connecticut, Storrs, CT, USA.

[5]Department of Genetics and Genome Sciences, University of Connecticut Health Center, Farmington, CT, USA.

[6]Institute for Systems Genomics, University of Connecticut, Farmington, CT, USA.

[7]Present address: Bristol-Myers Squibb, Pennington, NJ, USA.

[8]These authors contributed equally: Laura E. Mickelsen and Mohan Bolisetty.

Abstract

The lateral hypothalamic area (LHA) coordinates an array of fundamental behaviors, including sleeping, waking, feeding, stress and motivated behavior. The wide spectrum of functions ascribed to the LHA may be explained by a heterogeneous population of neurons, the full diversity of

which is poorly understood. We employed a droplet-based single-cell RNA-sequencing approach to develop a comprehensive census of molecularly distinct cell types in the mouse LHA. Neuronal populations were classified based on fast neurotransmitter phenotype and expression of neuropeptides, transcription factors and synaptic proteins, among other gene categories. We define 15 distinct populations of glutamatergic neurons and 15 of GABAergic neurons, including known and novel cell types. We further characterize a novel population of somatostatin-expressing neurons through anatomical and behavioral approaches, identifying a role for these neurons in specific forms of innate locomotor behavior. This study lays the groundwork for better understanding the circuit-level underpinnings of LHA function.

The LHA is critical in coordinating diverse physiological and behavioral functions, including sleep–wake states, feeding, stress and motivated behavior[1–3]. Underlying this functional diversity is a heterogeneous collection of neurons exhibiting complex cytoarchitecture[4]. The best known of these are small populations of neuropeptidergic neurons expressing hypocretin (also known as orexin; encoded by *Hcrt*) or melanin-concentrating hormone (encoded by *Pmch*), each of which potently influence innate behavior[1–6]. Other LHA neuronal populations have been described based on their expression of other neuropeptides, receptors and markers of the synthesis and/or packaging of the fast amino acid neurotransmitters GABA or glutamate[1–3]. Optogenetic and chemogenetic approaches have revealed LHA GABAergic (LHA^GABA) and glutamatergic (LHA^Glut) neurons to be robust actuators of arousal, feeding and motivated behavior[1–3,7]. It is likely that within these broad classes of neurons, there are molecularly distinct populations that differ in functional connectivity and behavioral state-dependent engagement. Yet, cellular heterogeneity among these populations remains poorly defined.

To provide a more comprehensive census of the cell-type diversity in the LHA, we applied a droplet-based single-cell RNA-sequencing (scRNA-seq) strategy to not only identify novel populations but also diversity among known ones. We validated differentially expressed genes through fluorescence in situ hybridization (FISH) and an orthogonal approach, single-cell quantitative PCR (sc-qPCR) profiling. Finally, our scRNA-seq data led us to probe the unique connectivity of a novel population of transcriptionally and topographically distinct LHA neurons and to examine their role in forms of innate behavior. Taken together, this analysis informs our understanding of the molecular basis of LHA cell-type heterogeneity and serves as the foundation for more refined circuit-specific interrogations of LHA function.

Results

Single-cell isolation and transcriptomic analysis of LHA cell populations.

To isolate LHA neurons for scRNA-seq analysis, we microdissected the LHA from fresh brain slices obtained from both male and female C57BL/6 mice (postnatal day (P) 30) as previously described[8] and processed single-cell suspensions through the 10× Genomics Chromium Controller (Fig. 1a). Microdissections were mapped for accuracy and reproducibility (Fig. 1b). Our initial clustering combined the single-cell expression data from male ($n = 3,784$ cells) and female ($n = 3,434$ cells) samples, and we found that each

cluster comprised cells from both genders, indicating that there were few sex-dependent differences (Supplementary Fig. 1). In our pooled dataset, the median number of genes per cell was 2,799, and the median number of transcripts (unique molecular identifiers (UMIs)) per cell was 6,079 (Fig. 1c). We used the top 1,000 genes based on normalized dispersion analysis for dimension reduction using t-distributed stochastic neighbor embedding (t-SNE) followed by cluster identification using density-based spatial clustering of applications with noise (DBSCAN), and identified 20 clusters. We separated neuronal and non-neuronal clusters based on the aggregated expression of the following four pan-neuronal markers: *Snap25* (encoding synaptosome associated protein 25), *Syp* (encoding synaptophysin), *Tubb3* (encoding tubulin, beta 3 class III) and *Elavl2* (encoding ELAV like RNA binding protein 1) (Fig. 1d,e). We found that the mean numbers of genes per cell and transcripts per cell were significantly lower in non-neuronal cells (mean number of genes (transcripts): 1,737 (4,156)) (Supplementary Fig. 2d) compared with neurons (mean number of genes (transcripts): 3,442 (8,791)) (Supplementary Fig. 3a,c), explaining the prominent bimodal distributions seen in Fig. 1c. Using unsupervised clustering, we identified 13 distinct populations (Supplementary Fig. 2a,b) among the non-neuronal cells, and most of these populations were defined by known cell type-specific discriminatory markers (Supplementary Fig. 2c).

Unsupervised clustering reveals a diversity of inhibitory and excitatory neuronal cell types.

We next used unsupervised, iterative clustering to distinguish molecularly distinct neuronal clusters. We first found a dichotomy among LHA neuronal clusters based on the expression of genes necessary for the synthesis and packaging of glutamate and GABA. In particular, *Slc17a6*, which encodes vesicular glutamate transporter 2 (VGLUT2), was expressed by a distinct collection of clusters (Fig. 1f). In contrast, another collection of clusters robustly expressed *Slc32a1*, which encodes vesicular GABA transporter (VGAT). The expression of genes encoding synthetic enzymes for GABA (*Gad1* (which encodes GAD67) and *Gad2* (which encodes GAD65)) largely tracked with *Slc32a1*⁺ clusters. Interestingly, *Gad2* expression better matched the *Slc32a1*⁺ pattern than *Gad1* expression (Fig. 1f). We nominally categorized *Slc17a6*⁺ clusters as glutamatergic and *Slc32a1*⁺ clusters as GABAergic (Fig. 1g).

A molecular census of LHA^Glut neurons.

LHA^Glut neurons were subdivided in an unsupervised manner into 15 distinct clusters (Fig. 2a,b), with each denoted by one to three markers. Notably, four *Slc17a6*⁺ and *Slc32a1*⁻ clusters robustly expressed *Gad1* (but not *Gad2*) (Figs. 1f and 2a,b), which were additionally denoted by *Gad1*. The number of cells, genes and UMIs detected for each cluster, and a heatmap of differential gene expression, are shown in Supplementary Fig. 3a,b and Supplementary Table 1. We next describe a selection of notable known and novel LHA^Glut populations that emerged from our classification scheme.

We identified a variety of LHA^Glut populations prominently expressing neuropeptides and other noteworthy markers. (1) Unsupervised clustering confirmed that *Hcrt*-expressing neurons (LHA^Glut cluster 6) represent a transcriptionally distinct population (Fig. 3;

Supplementary Fig 6). (2) Similarly, *Pmch*-expressing neurons (LHA[Glut] cluster 1) represent another distinct population (Fig. 4). (3) *Trh* (encoding thyrotropin-releasing hormone, TRH)-expressing neurons (LHA[Glut] clusters 8 and 12) represent another known population (Fig. 5). (4) *Tac1* (encoding tachykinin 1) is expressed by multiple LHA[GABA] and LHA[Glut] clusters, and in situ hybridization (ISH) data (Allen Mouse Brain Atlas)[9] show *Tac1* expression throughout the LHA (Supplementary Fig. 4). Notably, *Tac1* emerged as a top discriminatory marker for LHA[Glut] cluster 4 (expressing *Tac1* and *Pitx2* (encoding paired-like homeodomain transcription factor 2)) with selective expression of *Pitx2*. (5) LHA[Glut] cluster 10 selectively co-expresses *Grp* (encoding gastrin releasing peptide) and *Cck* (encoding cholecystokinin) transcripts, in addition to *Pdyn* (encoding prodynorphin) and *Nkx2–1* (encoding NK2 homeobox 1). ISH data show *Grp* (Supplementary Fig. 4) and *Cck* expression in the dorsomedial hypothalamus (DMH) and in rare cells in the LHA[9]. (6) LHA[Glut] cluster 11 is defined by the expression of *Calca* (encoding both calcitonin and calcitonin gene-related peptide), and enriched in *Col27a1* (encoding collagen type XXVII alpha 1), *Ebf3* (encoding early B cell factor 3), *Otp* (encoding orthopedia homeobox), *Tcf4* (encoding transcription factor 4) and *Nkx2–1* and *Cbln2* (encoding cerebellin 2 precursor protein). ISH data show a discrete cluster of *Calca*^{+} cells in the tuberal region[9] (Supplementary Fig. 4). (7) Another intriguing LHA[Glut] population is specified by *Synpr* (encoding synaptoporin) expression (LHA[Glut] cluster 9, *Synpr* with *Gad1*). ISH data show that *Synpr*^{+} cells are found scattered across the DMH and LHA[9] (Supplementary Fig. 4). (8) Glutamatergic somatostatin (*Sst*)-expressing neurons (LHA[Glut] cluster 15) co-express a host of discriminatory markers (Fig. 7; Supplementary Figs. 10 and 12).

A molecular census of LHA[GABA] neurons.

LHA[GABA] neurons were classified in an unsupervised manner into 15 distinct clusters (Fig. 2c,d), referred to by one or two markers. For each cluster, the number of cells, genes, and UMIs detected, and a heatmap of marker genes are presented in Supplementary Fig. 3c,d and Supplementary Table 1. An apparent outlier is cluster 4, which exhibits significantly lower gene and UMI counts and is therefore unassigned. Noteworthy known and novel LHA[GABA] populations are discussed.

We identified diverse LHA[GABA] populations defined by key markers. (1) We found two distinct but related populations expressing *Gal* (encoding galanin; LHA[GABA] cluster 1, *Gal* with *Dlk1* (encoding delta like non-canonical Notch ligand 1)) and *Nts* (encoding neurotensin; LHA[GABA] cluster 3, *Nts* with *Cartpt* (encoding cocaine- and amphetamine-regulated transcript)). Clusters 1 and 3 share high expression of *Dlk1*, but are distinguished by robust and selective co-expression of *Tac1*, *Calcr* (encoding calcitonin receptor) and *Cbln2* in cluster 3 (Fig. 2d). Further analysis of LHA *Nts*^{+} neurons is described in Fig. 6 and Supplementary Fig 8. (2) We identified three molecularly distinct populations of *Sst*-expressing LHA[GABA] neurons: clusters 6 (*Sst* with *Col25a1*), 10 (*Sst* with *Meis2*) and 13 (*Sst* with *Otp*), described in detail in Fig. 7 and Supplementary Figs. 10–12. (3) LHA[GABA] cluster 2 selectively expresses *Npy* (encoding neuropeptide Y), *Npw* and *Ebf1*. Previous work had identified a population of glucose-sensitive *Npy*-expressing LHA neurons[10] as well as *Npy* and *Npw* co-expressing neurons in the DMH and LHA[11]. In the latter study, co-expression peaked over the first three postnatal weeks but declined after P28. Our LHA[GABA]

cluster 2 (P30 mice) may represent the remainder of this distinct, although transient population. (4) LHA[GABA] cluster 12 (*Th* (encoding tyrosine hydroxylase) with *Slc18a2* (encoding vesicular monoamine transporter 2)) co-expresses markers of dopamine synthesis and packaging, *Th*, *Ddc* (encoding dopa decarboxylase) and *Slc18a2*. Scattered *Th*^{+} neurons have been identified in the rodent LHA[9,12] (Supplementary Fig. 4). (5) Another intriguing cluster co-expresses *Lhx6* (encoding LIM homeobox protein 6) and *Tcf4* (LHA[GABA] cluster 8). *Lhx6* defines a population of neurons found in this region[13,14].

Validation of key discriminatory markers for select populations of LHA[GABA] and LHA[Glut] neurons.

We next independently validated our data using FISH. We focused on *Hcrt*[+] (LHA[Glut] cluster 6), *Pmch*[+] (LHA[Glut] cluster 1), *Trh*[+] (LHA[Glut] clusters 8 and 12), *Nts*[+] (LHA[GABA] cluster 3) and *Sst*[+] (LHA[Glut] cluster 15; LHA[GABA] clusters 6, 10 and 13) clusters, as a cross-section of known and novel LHA populations. We also used an orthogonal approach, sc-qPCR of genetically labeled cells sorted via fluorescence-activated cell sorting (FACS), for several of these populations. For sc-qPCR, we used a curated panel of TaqMan probes (Supplementary Table 2), largely informed by our scRNA-seq analysis. We further predicted and validated the existence of subpopulations within defined clusters.

LHA[Glut] *Hcrt*-expressing neurons.

LHA *Hcrt*^{+} neurons constitute a well-described neuropeptidergic population, governing aspects of arousal, reward, stress and metabolism[1–5]. Our scRNA-seq analysis revealed a suite of discriminatory markers (Figs. 2b and 3a), including *Pdyn*, *Nptx2*, *Lhx9*, *Rfx4*, *Pcsk1*, *Nek7* and *Plagl1*. Other transcripts exhibited robust, but less selective, expression, including *Scg2*, *Cbln1*, *Vgf* and *Slc2a13*. Many of these markers had been previously identified in a bulk translating ribosome affinity purification (TRAP) analysis of mouse *Hcrt*^{+} neurons[15].

For sc-qPCR analysis, we FACS-sorted *Hcrt*^{+} neurons isolated from orexin–enhanced green fluorescent protein (Ox–EGFP) transgenic mice (Fig. 3b). Consistent with our scRNA-seq analysis, and previous results[8], *Hcrt*^{+} neurons exhibited very sparse expression of *Slc32a1* (4.0%) but widespread expression of *Slc17a6* (93.0%). Similarly, we confirmed that *Hcrt*^{+} neurons express *Scg2* (100%), *Slc2a13* (100%), *Nptx2* (99.0%) and *Nek7* (84.0%). Using FISH, we confirmed that *Hcrt* expression is restricted to the LHA, whereas *Slc2a13*, while strongly expressed in the LHA in addition to other regions, is detectable in the cortex and hippocampus as expected[9] (Supplementary Fig. 5a,b). FISH confirmed that a large proportion of *Hcrt*^{+} neurons co-expressed *Rfx4* (88.6%), *Nptx2* (99.5%) and *Pcsk1* (91.3%) (Fig. 3c), in addition to *Scg2* (100%) and *Slc2a13* (98.4%) (Supplementary Fig. 6a).

Previous studies have suggested that there is functional heterogeneity among *Hcrt*^{+} neurons, including diverse electrical and pharmacological signatures, projections and roles in diverse behaviors[1–5], which would be expected to manifest transcriptionally. We found that further subclustering of *Hcrt*^{+} neurons revealed two poorly defined subclusters, best distinguished by sex-specific genes, *Ddx3y* (subcluster 1) and *Xist* (subcluster 2), and an immediate-early gene, *Fos* (subcluster 1), among others (Supplementary Fig. 6b–d). These data suggest a role

for sexual dimorphism and/or activity in distinguishing subclusters. However, determining clear molecular heterogeneity among *Hcrt*^{+} neurons may require a larger sample size and a more systematic examination of the full *Hcrt*[+] field.

LHA[Glut] *Pmch*-expressing neurons.

LHA *Pmch*^{+} neurons (LHA[Glut] cluster 1) (Fig. 2a) represent another well-described population that is implicated in modulating sleep–wake states, metabolism and other functions[1–4,6]. A detailed analysis of *Pmch*^{+} neurons revealed a suite of known and novel markers (Figs. 2b and 4a), including *Cartpt, Tacr3, Chodl, Zic1, Otx1, Parpbp, Igf1, Pcdh8, Nptx1* and *Ntm*. Of note, *Zic1* is a novel marker, shared only with LHA[Glut] cluster 3, which interestingly shares other features with *Pmch*[+] LHA[Glut] cluster 1, including higher than baseline expression of *Pmch*, robust *Gad1* expression and moderate expression of *Cartpt, Cbln1* and *Nkx2–1*. These features suggest a distinct *Pmch*[+] subcluster or a cluster that shares a common developmental lineage.

Consistent with our scRNA-seq and previous data[8], sc-qPCR analysis of FACS-sorted *Pmch*^{+} cells showed ubiquitous expression of *Slc17a6* (100%), but undetectable *Slc32a1* (Fig. 4b). A large majority of *Pmch*^{+} neurons expressed *Ntm* (94.7%) and *Zic1* (94.7%). *Cartpt* and *Tacr3* were co-expressed in approximately one-third of *Pmch*^{+} neurons (Fig. 4b). FISH experiments confirmed that the population-wide markers *Zic1* (82.5%), *Chodl* (88.8%) and *Otx1* (97.1%) are enriched in *Pmch*^{+} neurons (Fig. 4c).

A subsequent iteration of clustering revealed that *Pmch*^{+} neurons may be parsed into two distinct subclusters (Fig. 4d). Some of the top discriminatory markers that identify *Pmch*^{+} neurons as a whole (Fig. 4a) appear to distinguish two subclusters (for example, *Cartpt, Tacr3, Parm1* and *Nptx1*, among others) (Fig. 4e). Subcluster 1 robustly and selectively expresses *Cartpt, Tacr3* and *Nptx1*, along with *Lypd1, Parm1* and *Amigo2*, among others. In contrast, subcluster 2 is better defined by the absence of *Cartpt*, with moderately selective expression of *Scg2* and *Nrxn3* (Fig. 4f).

We next validated these subclusters using triple-label FISH. Since *Cartpt* is a robust and selective marker for subcluster 1, we examined how the putative subcluster-specific markers *Tacr3, Nptx1* and *Nrxn3* segregated among *Pmch*[+] and *Cartpt*[+] (subcluster 1) and *Pmch*[+] and *Cartpt*[−] (subcluster 2) populations (Fig. 4g). Among *Pmch*[+] and *Cartpt*^{+} neurons, we found high co-expression with *Tacr3* (71.1%) and *Nptx1* (69.0%). In contrast, *Nrxn3* exhibited much lower co-expression among *Pmch*[+] and *Cartpt*^{+} neurons (28.0%). These data demonstrate that *Pmch*^{+} neurons may be parsed into two distinct subclusters with unique signatures.

This striking dichotomy among *Pmch*^{+} neurons supports previous neuroanatomical work. Approximately half of rat MCH neurons have been shown to co-express *Cartpt*[16,17], while the neurokinin 3 receptor (encoded by *Tacr3*) is co-expressed in *Cartpt*^{+} MCH neurons[18,19]. Furthermore, these two *Pmch*[+] subpopulations have differential birth order and projection patterns[18,19]. Our scRNA-seq, sc-qPCR and FISH analyses of *Pmch*-expressing neurons largely substantiates this dichotomy and sheds new light on the molecular distinctiveness of these subpopulations.

LHA^{Glut} *Trh*-expressing neurons.

We identified *Trh*-expressing neurons in the LHA, consistent with previous work[12,17]. We further revealed two distinct populations: *Trh* with *Cbln2* (LHA^{Glut} cluster 8) and *Trh* with *Syt2* (LHA^{Glut} cluster 12) (Fig. 2a,b and 5a). Both populations robustly express *Otp* and *Onecut2*, suggesting a common developmental lineage. *Otp* and *Onecut2* exhibit binary expression patterns among populations of LHA^{Glut} neurons, and in the case of *Onecut2*, expression is robust and unique to the two *Trh*+ populations, while *Otp* is expressed by four other LHA^{Glut} populations. *Asic4*, *Sall3*, *Mdga1* also exhibit high expression in both populations. FISH confirmed that the population-wide markers *Slc17a6* (93.6%), *Otp* (80.7%) and *Onecut2* (67.9%) are expressed in a large majority of *Trh*+ neurons (Fig. 5b).

A comparison of LHA^{Glut} clusters 8 and 12 revealed a host of differentially expressed transcripts (Fig. 5c,d). The markers that identify *Trh*+ cluster 8 neurons included *Cbln2* and *Gpr101*, whereas *Syt2* and *Cplx1* defined cluster 12 (Fig. 5e). Two of these transcripts (*Syt2* and *Cbln2*), each predicted to be unique to one or the other *Trh*+ cluster, were used in validation assays using triple-label FISH. Among *Trh*+ neurons that expressed *Syt2* and/or *Cbln2*, only 11.5% expressed both, while 33.4% expressed only *Syt2* and 55.1% expressed only *Cbln2* (Fig. 5f). The proportions of these two subpopulations appear to vary across the LHA rostrocaudal axis. *Trh*+ and *Syt2*+ neurons predominate anteriorly, while *Trh*+ and *Cbln2*+ neurons predominate posteriorly (Supplementary Fig. 7). Together, these data suggest that the transcripts encoding two synaptic proteins discriminate two molecularly distinct *Trh*+ populations.

LHA^{GABA} *Nts*- and *Cartpt*-expressing neurons.

We identified a *Nts*-expressing population (LHA^{GABA} cluster 3) that is characterized by robust co-expression with *Cartpt*. Analysis of *Nts*- and *Cartpt*-expressing neurons revealed other markers, including *Gal*, *Calcr*, *Rasgrp1*, *Acvr1c*, *Serpina3n*, *Crem*, *Gpr101* and *Jak1* (Figs. 2d and 6a). Cluster 3 neurons also exhibited minimal expression of *Slc17a6* and robust expression of *Slc32a1*, *Gad1* and *Gad2* (Fig. 2d), suggesting a conventional GABAergic phenotype, consistent with previous work[20]. Notably, LHA^{GABA} cluster 1 (*Gal* with *Dlk1*) neurons also expressed *Nts* (Fig. 2d) in addition to *Dlk1*, common to clusters 1 and 3 (Supplementary Fig. 8a,b). We next FACS-sorted *Nts*+ LHA neurons from *Nts*-Cre;EYFP (enhanced yellow fluorescent protein) mice for sc-qPCR (Fig. 6b). We found that the majority of sorted *Nts*+ neurons expressed *Jak1* (98.6%), *Gpr101* (79.5%) and *Gal* (67.1%), while *Cartpt* was expressed in 45.2% of *Nts*+ neurons. Although the large majority of sorted *Nts*+ neurons expressed *Slc32a1* (78.1%) as expected, we also found that a proportion of *Nts*+ neurons instead expressed *Slc17a6* (26.0%). Although *Nts* did not emerge as a discriminatory marker for any single LHA^{Glut} cluster in our scRNA-seq analysis, *Nts*+ neurons were thinly dispersed among multiple LHA^{Glut} clusters, suggesting the presence of nominally glutamatergic *Nts*+ neurons in the region, perhaps accounting for our unexpected sc-qPCR results. To quantify this in our scRNA-seq data, we binarized the expression of *Nts* using a Gaussian mixture model, counted the number of *Nts*+ cells and found that 70.8% were GABAergic and 29.2% were glutamatergic, similar to our sc-qPCR data (Supplementary Fig. 8c,d).

Further validation of *Nts*+ neurons by FISH indicated that a majority of *Nts*+ neurons expressed *Gpr101* (68.5%) and *Jak1* (78.7%) (Fig. 6c). In contrast, *Cartpt* was found in only 18.1% of *Nts*+ neurons (Fig. 6c). To address this discrepancy, we binarized the expression of *Nts* and *Cartpt* in our scRNA-seq data and found that LHA^{GABA} cluster 3 *Nts*+ and *Cartpt*+ co-expressing neurons actually constitute only 19.5% of all *Nts*+ cells in our dataset (Supplementary Fig. 8c,d), corroborating our FISH data. Together, these data support our conclusion that *Nts* and *Cartpt* co-expression is a unique molecular signature for a subset of LHA *Nts*+ GABAergic neurons. Finally, we found that the proportion of *Nts*+ neurons co-expressing *Cartpt* varies across the rostrocaudal axis of the LHA, with the greatest degree of co-expression found in the mid-LHA (Supplementary Fig. 8e).

A second iteration of clustering revealed that the *Nts*+ and *Carpt*+ population itself could be parsed into two distinct subclusters (1 and 2) (Fig. 6d,e). Although *Gal* expression did not discriminate between subclusters, *Crh* defined subcluster 1 while *Tac1* defined subcluster 2 (Fig. 6f). Triple-label FISH indicated *Gal* co-expression in 59.0% of *Nts*+ and *Slc32a1*+ neurons, but was undetectable among *Nts*+ and *Slc32a1*− neurons (Fig. 6g), underscoring the selectivity of *Nts* and *Gal* co-expression for LHA^{GABA} populations. Among *Nts*+ neurons that expressed *Tac1* and/or *Crh*, only 9.9% expressed both, while 50.4% expressed only *Tac1* and 39.7% only *Crh* (Fig. 6g), indicating that they define largely mutually exclusive populations. These data suggest that even unique clusters of LHA^{GABA} neurons may be diverse.

LHA neurons expressing *Nts* and *Gal* have been shown to exhibit significant co-expression of the long isoform of the leptin receptor (LepRb, encoded by *Lepr*) and the melanocortin-4 receptor (MC4R, encoded by *Mc4r*)[20–23]. Surprisingly, we found that *Nts*+ LHA^{GABA} cluster 3 neurons, and LHA^{GABA} neurons generally, exhibited low or sparse expression of *Lepr* and *Mc4r* (Supplementary Fig. 9a). A recent scRNA-seq analysis of hypothalamic regions known to be enriched in *Lepr*-expressing neurons implicated in energy balance also revealed similarly low expression of *Lepr*[24]. We performed sc-qPCR on FACS-sorted LHA neurons from *Lepr*-Cre;EYFP mice (Supplementary Fig. 9b,c) and found that a large majority of *Lepr*-expressing LHA neurons exhibited a GABAergic phenotype (*Slc32a1*+, *Gad1*+ and *Gad2*+) and are enriched in *Nts*, *Gal* and *Cartpt* transcripts, broadly substantiating previous anatomical analyses[20–23].

Multiple transcriptionally distinct *Sst*-expressing populations.

We defined the following four *Sst*+ populations in the LHA: LHA^{Glut} cluster 15 (*Sst*); and LHA^{GABA} clusters 6 (*Sst* with *Col25a1*), 10 (*Sst* with *Meis2*) and 13 (*Sst* with *Otp*). *Sst* has been shown to be expressed in multiple hypothalamic regions, including perikarya in the LHA[9,12,25], but little is known of their anatomy or function. Our bioinformatic analysis revealed a host of discriminatory markers. *Sst*+ LHA^{Glut} cluster 15 exhibited high expression of *Ebf3*, *Tcf4* and *Nkx2–1* (Fig. 2b) and selective expression of *4833423E24Rik*, *Prokr1* and *Prlr* (Fig. 7a). This cluster is also unique in expressing transcripts for *Npy* and *Npw*, the co-expression of which curiously defines LHA^{GABA} cluster 2 (Fig. 2a). *Sst*+ LHA^{GABA} cluster 6 is distinguished by its robust expression of *Col25a1*, *Otp* and *Cbln4* (Figs. 2b and 7b). Cluster 10 exhibited high expression of *Meis2*, *Cbln2*, *Dlk1*, *Tac1*, *Calb2* and *Gda* (Figs. 2b

and 7b). Cluster 13 is characterized by *Otp*, *Dlk1*, *Calb1*, *Ptk2b*, *Pthlh*, *Nrgn*, *Rprml* and *Icam5* (Figs. 2b and 7b).

To better understand the suite of markers that differentiate these four populations, we subjected all *Sst*^{+} neurons in our dataset to iterative clustering. We confirmed the primary dichotomy within this population was fast neurotransmitter phenotype (Fig. 7c) along with markers that drive this separation. The *Slc32a1*[+] population parsed into three distinct clusters (Fig. 7d), recapitulating our initial clustering (Fig. 7e).

We next determined whether we could detect both the predicted glutamatergic and GABAergic *Sst*[+] populations from genetically labeled *Sst*^{+} neurons using sc-qPCR. We found that the majority of FACS-sorted *Sst*^{+} LHA neurons (from *Sst*-Cre;EYFP mice) (Fig. 7f) expressed *Slc32a1* (73.6%). However, a largely mutually exclusive population expressed *Slc17a6* (32.6%), consistent with our scRNA-seq data. *Meis2*, a discriminatory marker for *Sst*[+] LHA[GABA] cluster 10, was expressed in 51.7% of all *Sst*^{+} neurons, enriched among *Sst*[+] and *Slc32a1*^{+} neurons, and virtually undetectable among *Sst*[+] and *Slc17a6*^{+} neurons, as predicted. Transcripts for *Npy* and *Npw*, however, were virtually absent among *Sst*[+] and *Slc17a6*^{+} neurons (Fig. 7f).

Next, we performed triple-label FISH to validate the predicted fast neurotransmitter markers for *Sst*^{+} LHA neurons. In our initial FISH detection of LHA *Sst*^{+} neurons, we observed relatively sparse *Sst*[+] cell bodies in the perifornical LHA and a higher concentration of *Sst*[+] cell bodies in the adjacent tuberal region in more posterior sections (Fig. 7g). We first asked whether *Sst*^{+} neurons with glutamatergic or GABAergic phenotypes are differentially distributed between these two regions. Using FISH, we found that *Sst*^{+} neurons in the perifornical LHA were 56.1% *Slc32a1*[+], 43.6% *Slc17a6*[+] and 0.3% *Slc17a6*[+] and *Slc32a1*[+] (Fig. 7g), a proportion that varied across the rostrocaudal axis, with up to 71.1% of *Sst*^{+} neurons being *Slc17a6*[+] in posterior regions (Supplementary Fig. 10a). In contrast, *Sst*^{+} neurons in the tuberal region were 1.6% *Slc17a6*[+], 97.3% *Slc32a1*[+] and 1.1% *Slc17a6*[+] and *Slc32a1*[+] (Fig. 7g), a proportion that remained relatively constant in middle and posterior tuberal regions (Supplementary Fig. 10b).

We next examined whether other discriminatory markers for specific *Sst*[+] populations exhibit differential topography across subregions. We first examined the distribution of the following four markers of *Sst*[+] and *Slc32a1*[+] LHA[GABA] populations: *Meis2*, *Otp*, *Ptk2b* and *Nrgn*. *Meis2*, a marker of LHA[GABA] cluster 10 neurons, was expressed in 50.4% of perifornical *Sst*[+] and *Slc32a1*^{+} neurons (Supplementary Fig. 11a), but undetectable among their tuberal counterparts (Supplementary Fig. 11b). In contrast, *Otp*, *Ptk2b* and *Nrgn* were distributed to varying degrees among *Sst*[+] and *Slc32a1*^{+} neurons between the two regions (Supplementary Fig. 11a,b). We next examined the distribution of the following three markers of the *Sst*[+] and *Slc17a6*[+] LHA[Glut] population among perifornical neurons: *Nkx2–1, Npy* and *Calcr*. *Nkx2–1, Npy* and *Calcr* were expressed in only 7.8, 5.8 and 12.6%, respectively, of *Sst*[+] and *Slc17a6*^{+} neurons (Supplementary Fig. 12a). This result indicates that they are either poor markers for *Sst*[+] LHA[Glut] neurons or are largely expressed below the detection limit of FISH. Taken together, these data suggest that in the perifornical LHA, *Sst*^{+} neurons represent a mix of GABAergic (LHA[GABA] clusters 6, 10 and 13) and

glutamatergic (LHA^{Glut} cluster 15) Sst^+ populations, whereas in the tuberal region, only LHA^{GABA} clusters 6 and 13 are present, given the absence of $Meis2^+$ cluster 10 neurons.

As a step toward functional characterization of LHA Sst^+ neurons, we next considered whether Sst^+ neurons in the perifornical LHA and tuberal region may be distinguished by electrophysiological signatures. We systematically subjected both perifornical and tuberal EYFP$^+$ neurons from Sst-Cre;EYFP mice to a battery of whole-cell voltage-clamp and current-clamp protocols to assess passive and active membrane properties, while mapping their location within the slice (Supplementary Fig. 13a,b). We found that EYFP$^+$ neurons in the perifornical region had significantly shorter action potential half-widths, faster decay times and deeper afterhyperpolarization amplitudes than their tuberal counterparts (Supplementary Fig. 13c,d). Furthermore, EYFP$^+$ perifornical neurons exhibited significantly lower repolarization latencies and faster maximal firing rates than tuberal neurons (Supplementary Fig. 13e–g). These data demonstrate that Sst^+ neurons in the perifornical LHA and tuberal region exhibit quantifiably different intrinsic membrane properties, consistent with topographical differences in the proportions of transcriptionally distinct Sst^+ neuronal populations.

Role for LHA Sst^+ neurons in repetitive locomotor behavior.

To explore the potential role for the broad population of LHA Sst^+ neurons within the spectrum of innate behaviors associated with LHA function, we pursued a chemogenetic strategy to selectively activate genetically defined LHA Sst^+ neurons while monitoring behavior. Recent work has demonstrated that activation of LHA^{GABA} and LHA^{Glut} neurons induces profound effects on consummatory behavior, reward and arousal[1–3,7]. We determined whether selective activation of LHA Sst^+ neurons could recapitulate any of these behavioral phenotypes. We targeted the Gq-linked excitatory designer receptor exclusively activated by designer drugs (DREADD), hM3Dq, to LHA Sst^+ neurons using a Cre-dependent hM3Dq virus (AAV-DIO-hM3Dq-mCherry) or control virus (AAV-DIO-mCherry) in Sst-Cre mice (Fig. 8a). This allowed us to specifically activate LHA Sst^+ neurons with systemic clozapine-N-oxide (CNO) during a video-based behavioral screen. Post hoc validation of viral expression in LHA Sst^+ neurons was assessed to verify that the injection was localized within the boundaries of the LHA (Fig. 8a; Supplementary Fig. 14a,b). c-Fos immunoreactivity was also assessed to show that hM3Dq-mCherry$^+$ neurons were selectively activated following CNO administration (Supplementary Fig. 14c). Mice were habituated to the chamber environments before injection with CNO (1 mg per kg, intraperitoneally) (Fig. 8b). Experiments were performed early in the light/inactive period to evaluate possible arousal-related activity. For each condition, we compared the 1 h period before injection (pre-injection) and a 1 h period following injection (post-injection) (Fig. 8b).

We first monitored locomotor activity, measured as distance traveled (m), using both center-point and nose-point detection. We found that hM3Dq mice exhibited a striking and significant enhancement in locomotor activity relative to control animals, which were often resting during a period of high sleep-pressure (Fig. 8c). To assess the nature of this enhanced locomotor activity on a finer scale, we used side-mounted cameras to monitor and manually

score the following ten discrete behaviors: resting, rearing, walking, grooming, eating, drinking, nestlet shredding, digging, gnawing and nest activity (Fig. 8b). Transitions between behaviors were assessed for each control and hM3Dq mouse and represented in color-coded heatmaps (Fig. 8d) as well as a representation of total cumulative time spent engaged in each behavior in the post-injection period (Fig. 8e). We found that relative to control mice, hM3Dq mice exhibited a significant reduction in resting and significant increases in rearing, digging, eating and gnawing following CNO injection (Supplementary Fig. 14d,e). One of these elicited behaviors was repetitive gnawing and biting of wooden objects in the chamber (Fig. 8f; Supplementary Fig. 14e), which some animals would engage in persistently for minutes at a time. These data suggest that selectively activating LHA *Sst*$^+$ neurons elicits specific locomotor activities during a normally inactive period, in addition to modest increases in consummatory and exploratory behavior. These results are reminiscent of a subset of the behavioral phenotypes observed during activation of the broad population of LHA^{GABA} neurons[26–33].

A unique projection target of LHA^{Glut} *Sst*$^+$ neurons.

As a first step toward a circuit-level understanding of the complex behavioral phenotype we observed in our chemogenetic screen of LHA *Sst*$^+$ neurons, we determined where single, transcriptionally distinct *Sst*$^+$ neuron populations project in the brain. To this end, we focused on the projection targets of LHA^{Glut} *Sst*$^+$ (cluster 15) neurons, uniquely found in the perifornical LHA, and asked if there are regions of the brain that both LHA *Sst*$^+$ neurons and LHA^{Glut} neurons project to, but LHA^{GABA} neurons do not. To accomplish this, we carried out stereotactic injections of an anterograde Cre-dependent virus (AAV-DIO-ChR2-EYFP) into the LHA of *Sst*-Cre, *Vgat*-Cre and *Vglut2*-Cre mice (Fig. 8g). In our examination of long-range projections of LHA *Sst*$^+$ neurons, we found particularly dense fibers in the region of the dorsal lateral septal nuclei (dLS) (Fig. 8h). Examination of the dLS in *Vglut2*-Cre mice revealed similarly dense fibers, whereas we found only sparse fibers in the dLS of *Vgat*-Cre mice (Fig. 8h). To test our inference that LHA^{Glut} *Sst*$^+$ neurons may preferentially project to the dLS, we carried out retrograde tracing experiments. We stereotactically injected the dLS with cholera toxin subunit b (CTb), resolved retrogradely labeled neurons in the LHA using an anti-CTb antibody, combined with FISH for *Sst* and either *Slc32a1* or *Slc17a6* in both the perifornical and tuberal regions (Fig. 8i). In the perifornical LHA, we found that whereas 16.4% of CTb-immunoreactive and *Sst*$^+$ neurons were *Slc32a1*$^+$, a striking 75.3% were *Slc17a6*$^+$. In the tuberal region, 15.0% of CTb-immunoreactive and *Sst*$^+$ neurons were *Slc17a6*$^+$ and 51.1% were *Slc32a1*$^+$ (Fig. 8j). Taken together, these data suggest that LHA^{Glut} *Sst*$^+$ neurons found in the perifornical LHA preferentially innervate the dLS.

Discussion

We provide the first comprehensive single-cell transcriptome profiling of cell types within the mouse LHA. Using droplet-based scRNA-seq, we developed a molecular census of 11 non-neuronal, 15 GABAergic and 15 glutamatergic neuronal cell types. This census provides a detailed resource for precisely deconstructing the biology of genetically defined

LHA circuits and their orchestration of innate behavior. Key biological insights gleaned from these data are summarized below.

We found that neuronal clusters can be classified based on a confluence of markers that encode neurochemical phenotype, transcription factors and synaptic proteins, among other gene categories. These combinations of markers seem to specify the identity of transcriptionally distinct populations of LHA neurons, most likely reflecting a convergence of developmental lineage, neurochemistry and functional connectivity. Along with a broad dichotomy among clusters based on expression of *Slc32a1* and *Slc17a6*, many clusters were also defined by co-expression of neuropeptide transcripts, suggesting co-transmission. Although demonstrated in *Hcrt*^{+} neurons[34], our data predict widespread neuropeptide and fast neurotransmitter co-transmission among LHA cell types.

A host of transcription factors and transcriptional regulators also emerged as key discriminatory markers for populations of LHA neurons. An interesting example is *Meis2*, which is uniquely associated with a single LHA^{Glut} cluster and three LHA^{GABA} clusters, including one *Sst*[+] LHA^{GABA} population. *Meis2* was recently identified as a subtype-specific marker for a novel population of *Sst*[+] and *Slc17a6*^{+} neurons in the entopeduncular nucleus of the basal ganglia[35]. Likewise, *Lhx6*, which we identified as a marker of LHA^{GABA} cluster 8 neurons, defines a population of neurons in the LHA, DMH and ventral zona incerta (VZI)[13]. Recent evidence suggests that *Lhx6*-expressing GABAergic VZI neurons are sleep-promoting[14]. Finally, transcripts for proteins implicated in synaptic structure and function figure prominently as discriminatory markers. For example, *Syt2* and *Cplx1* are markers for a single LHA^{Glut} *Trh*[+] cluster. These synaptic markers suggest cell type-specificity in synapse formation, maintenance and neurotransmitter release.

Importantly, we found diversity among LHA^{Glut} and LHA^{GABA} neurons, which may explain the manifold behavioral effects elicited through optogenetic or chemogenetic manipulations. For example, activation of LHA^{GABA} neurons has been reported to elicit robust consummatory and reward-related behavior[29], in part mediated by a dense projection to the ventral tegmental area[26,27,30,31], and vigorous predatory behavior through projections to the periaqueductal gray[36]. Activation of LHA^{GABA} neurons was also shown to induce rapid wakefulness, arousal-related behavior and locomotion[7,32,33]. Other studies of this large population have revealed heterogeneity in electrical signatures[37] and activity during various behavioral states[29,38]. In particular, we provide molecular insight into distinct populations of *Gal*- and *Nts*-expressing LHA^{GABA} neurons, previously shown to exhibit significant co-expression with LepRb[20,21,23] and MC4R[22]. These populations have been implicated in feeding, energy balance, reward and stress[20–23,39–42]. Selective activation of neuropeptide-defined LHA^{GABA} populations, targeting *Gal*- or *Nts*-expressing neurons, revealed both divergent and overlapping behavioral phenotypes[40–42]. Our present work reveals avenues for future circuit-level dissection as a way of resolving the complex functional identity of these populations.

In turn, optogenetic activation of LHA^{Glut} neurons produces aversive responses and suppresses feeding behavior[26,27,43], mediated in part by a prominent projection to the lateral habenula[44]. Recent work also suggests that LHA^{Glut} projections to the periaqueductal gray

mediate behavioral evasion[36]. In addition to well-described *Hcrt*[+] and *Pmch*^{+} neurons, we identified several intriguing excitatory populations, including two clusters of *Trh*-expressing neurons. Hypothalamic TRH has been implicated in arousal, feeding behavior, thermogenesis and metabolism through its role in the hypothalamic–pituitary–thyroid axis[45]. A possible role for LHA *Trh*^{+} neurons in feeding behavior is underscored by the observation that they are innervated by arcuate nucleus agouti-related neuropeptide and pro-opiomelanocortin neurons[12]. Further work will be required to determine how these and other LHA[Glut] populations, revealed by our scRNA-seq analysis, underlie aversive or evasive phenotypes observed at the behavioral level.

Finally, through anatomical and functional analyses, we explored the biology of a novel population of LHA *Sst*^{+} neurons, which have been detected in the LHA[9,12,25] but are poorly understood. Our behavioral data are generally consistent with a growing body of literature describing arousal, consummatory and exploratory behaviors associated with the activation of LHA[GABA] neurons in mice[26–33]. Gnawing or biting non-food items, in addition to food consumption, was observed in early LHA stimulation experiments[1–3]. More recently, gnawing behavior was also observed following activation of LHA[GABA] neurons[31] as well as more selective activation of LHA[GABA], but not LHA[Glut], fibers innervating the ventral tegmental area[26]. Interestingly, recent work demonstrated that optogenetic activation of the central nucleus of the amygdala, and its projections to the hindbrain, elicits a similar gnawing and biting of non-food items, suggestive of a consummatory-like locomotor program, separate from actual food consumption[46]. Furthermore, the dLS, and their projections to the LHA, have also been implicated in food-seeking behavior, independent of food consumption[47]. Most recently, optogenetic activation of *Sst*-expressing GABAergic neurons in the tuberal region have been shown to elicit feeding[48]. The circuit-level mechanisms underlying the relationship between the transcriptionally diverse populations of LHA *Sst*^{+} neurons we identified, and the diverse behaviors observed in our chemogenetic screen, remain topics for future investigation.

In summary, our scRNA-seq classification of LHA cell types is a starting point for a more refined mapping of LHA inputs and outputs and a resource for circuit-specific interrogation of LHA function. These data, along with other recent hypothalamic scRNA-seq analyses[24,49,50], broaden opportunities for better understanding the complex molecular, synaptic and circuit-level mechanisms underlying hypothalamic function in health and disease states.

Methods

Ethics statement.

All experiments were performed in accordance with the ethical guidelines described in the National Institutes of Health's Guide for the Care and Use of Laboratory Animals and were approved by the Institutional Animal Care and Use Committee of the University of Connecticut and of the Jackson Laboratory (JAX) for Genomic Medicine.

Animals.

To isolate LHA neurons for scRNA-seq analysis, we used both male and female C57BL/6 (JAX stock no. 000664) mice. To sort putative genetically defined, fluorescently labeled LHA neuronal cell types using FACS, we used the following Cre recombinase driver lines, each of which was crossed to the EYFP reporter line B6.Cg-Gt(ROSA)26Sor[tm3(CAG-EYFP)Hze]/J (Ai3)[51] (JAX stock no. 007903), which selectively expresses EYFP following Cre-dependent recombination. (1) *Pmch*-Cre transgenic mice (Tg(Pmch-cre)1Lowl/J)[52] (JAX stock no. 014099) crossed to Ai3; *Pmch*-Cre;EYFP. (2) *Nts*-Cre knock-in mutant mice (B6;129-Nts[tm1(cre)Mgmj]/J)[20] (JAX stock no. 017525) crossed to Ai3; *Nts*-Cre;EYFP. (3) *Sst*-IRES-Cre knock-in mutant mice (Sst[tm2.1(cre)Zjh]/J)[53] (JAX stock no. 013044) crossed to Ai3; *Sst*-IRES-Cre;EYFP. (4) *Lepr*-Cre knock-in mutant mice (Lepr[tm3(cre)Mgmj])[54], provided by M. G. Jr Myers (University of Michigan), crossed to Ai3; *Lepr*-Cre;EYFP. (5) We also used Ox-EGFP transgenic mice in which the human prepro-orexin promoter drives the expression of EGFP[55,56], provided by T. Sakurai (University of Tsukuba). For anterograde tracing experiments, we additionally used the following mutant mice: (1) *Slc32a1*[tm2(cre)Lowl]/J knockin mice[57] (JAX stock no. 016962; referred to here as *Vgat*-Cre mice) to label *Slc32a1*-expressing GABAergic neurons; and (2) *Slc17a6*[tm2(cre)Lowl]/J knockin mutant mice[57] (JAX stock no. 016963, referred to here as *Vglut2*-Cre mice) to label *Slc17a6*-expressing glutamatergic neurons. All mice were fed ad libitum and kept on a 12 h light–dark cycle.

Brain slice preparation for microdissection and single-cell dissociation.

Single-cell dissociations for both scRNA-seq and sc-qPCR experiments were performed on microdissected LHA tissue from juvenile (P25–P32) mouse brain slices following previously described procedures[8]. All mice were killed by rapid decapitation following isofluorane anesthesia, within the same time period (morning, 9:00–11:00). We then obtained 225 μm thick slices using a vibrating microtome (Campden Instruments) in ice-cold, sucrose slicing solution containing the following components (in mM): 87 NaCl, 75 sucrose, 25 glucose, 25 NaHCO$_3$, 1.25 NaH$_2$PO$_4$, 2.5 KCl, 7.5 MgCl$_2$, 0.5 CaCl$_2$ and 5 ascorbic acid saturated with 95% O$_2$/5% CO$_2$. Slices were enzyme-treated for ~15 min at 34 °C using protease XXIII (2.5 mg ml^{-1}; Sigma) in a sucrose dissociation solution containing the following components (in mM): 185 sucrose, 10 glucose, 30 Na$_2$SO$_4$, 2 K$_2$SO$_4$, 10 HEPES buffer, 0.5 CaCl$_2$ 6 MgCl$_2$, 5 ascorbic acid (pH 7.4) and 320 mOsm. Slices were washed three times with cold dissociation solution then transferred to a trypsin inhibitor/ bovine serum albumin (BSA) solution (1 mg ml^{-1}; Sigma) in cold sucrose dissociation solution. Three to four slices were obtained from each animal that approximately corresponded to mouse brain atlas images representing the distance from bregma −1.34 mm, −1.58 mm and −1.82 mm[58], which included the LHA region caudal to the retrochiasmatic area and rostral to the tuberomammillary nucleus in the posterior hypothalamus. The region we define as the LHA corresponds to the caudal portion of the LHA and portions of the tuberal nucleus as described in the Allen Mouse Brain Atlas[9], or to the peduncular part of the lateral hypothalamus, medial tuberal nucleus and terete hypothalamic nucleus described in Paxinos and Franklin (2012)[58]. The LHA was microdissected bilaterally from appropriate slices using both a circular 1.0-mm diameter disposable biopsy punch (Ted Pella) as well as iridectomy scissors. Using a dissecting microscope, the tissue punch was positioned to

excise the region of the LHA from each slice, based on visual identification of the following key anatomical landmarks: ventral to the mammillothalamic tract, ventromedial to the cerebral peduncle, lateral to the DMH, dorsolateral to the ventromedial nucleus of the hypothalamus and including the fornix in the ventromedial quadrant of each punch. In addition to the circular tissue punch, we used iridectomy scissors to remove the ventrolateral subdivision of each LHA slice, which includes the tuberal nucleus and medial tuberal nucleus. Each microdissected brain slice was then photographed using the dissecting microscope, and the borders of the tissue punch were subsequently mapped onto mouse atlas images[58] (Fig. 1b). All microdissections were confined to the LHA, but in some cases may also include portions of the VZI and/or lateral portions of the DMH, as indicated in Fig. 1b. Microdissected tissue punches were kept in sucrose dissociation solution (with trypsin inhibitor/BSA) on ice until trituration. Immediately before dissociation, tissue punches were incubated for ~10 min in a 37 °C water bath, then triturated with a series of small bore fire-polished glass Pasteur pipettes in a volume of 400–600 μl trypsin inhibitor/BSA sucrose dissociation solution. Single-cell suspensions were passed through 60 μm nylon mesh filters to remove any cell aggregates, and kept on ice until single-cell capture.

scRNA-seq cell capture and sequencing.

For scRNA-seq experiments, hypothalamic brain slices that included the LHA were obtained from three male (pooled) and two female (pooled) juvenile C57BL/6 mice (P30), all of which were littermates. The viability of each single-cell suspension was assessed using a Countess II FL Automated Cell Counter (Thermo Fisher Scientific). Suspensions of dissociated cells were filtered through 20 μm nylon mesh filters to remove cell aggregates and large debris and were loaded onto independent single channels of a Chromium Controller (10× Genomics) single-cell platform. Briefly, ~12,000 single cells were loaded for capture using a Chromium Single Cell 3′ Reagent kit, v2 Chemistry (10× Genomics). Following capture and lysis, complementary DNA was synthesized and amplified (14 cycles) as per the manufacturer's protocol (10× Genomics). The amplified cDNA was used to construct an Illumina sequencing library and sequenced on a single lane of a HiSeq 4000 (Illumina). For FASTQ generation and alignments, Illumina basecall files (*.bcl) were converted to FASTQs using Cell Ranger v.1.3 (10× Genomics), which uses bcl2fastq v.2.17.1.14. FASTQ files were then aligned to mm10 genome and transcriptome using the Cell Ranger v.1.3 pipeline, which generates a 'gene vs cell' expression matrix. Male and female matrices were merged using Cell Ranger aggregate pipeline.

scRNA-seq analysis.

For filtering and unsupervised clustering, the gene expression matrix from Cell Ranger was used for downstream analysis (using Python 2.7.8 and R 3.3.1). Of the initial 7,218 cells (3,784 male and 3,434 female), 89 cells with less than 500 UMIs or >40% of mitochondrial reads were discarded. Genes with at least 2 counts in 5 cells were used for downstream analysis. Gene expression of the remaining 7,129 cells was normalized by the total number of transcripts detected in each cell and multiplied by the median transcript count. The normalized expression was $\log_2$-transformed after an addition of a pseudocount. The top 1,000 genes with the most variance were identified based on their mean expression in the population and dispersion (variance/mean expression). Genes were binned into 50 different

bins based on their mean expression and dispersion scaled with respect to the median dispersion in each bin. These genes were used to reduce the dimensions of the dataset using Barnes Hut t-SNE with default parameters. Cells were clustered in t-SNE space using DBSCAN. In each case, this was through an iterative process, testing different parameters and visualizing ellipse thresholds to ensure that clusters were optimally resolved into distinct units in t-SNE space. In the case of male and female samples, both sexes were combined for the analysis. The calculation for the top 1,000 genes, dimensionality reduction and clustering were performed on a combined gene expression matrix, which led to a single representation of cells in t-SNE space.

To differentiate neuronal and non-neuronal clusters, the entire gene vs cell matrix was filtered and clustered as described above. This identified 20 initial clusters. To classify a cluster as a neuron or a non-neuron cluster, we aggregated the median expression of the known neuron markers *Snap25*, *Syp*, *Tubb3* and *Elavl2* for each cluster. We aggregated the median expression of these genes in each cluster and classified a cluster as high (neuronal) or low (non-neuronal) expression using a simple Gaussian mixture model. Every cell was then classified as a neuron or non-neuron based on their cluster membership. A total of 185 cells were discarded as they were present in clusters classified as both neuronal and non-neuronal. Subsequent clustering of non-neuronal and neuronal populations was based on this classification. For classification of GABAergic and glutamatergic clusters, clusters classified as neurons were combined and re-clustered as described above, which yielded 30 clusters. Clusters were classified as GABAergic if the median expression of *Slc32a1* is greater than *Slc17a6* in each cluster and glutamatergic if the median expression of *Slc17a6* is greater than *Slc32a1* (Fig. 3). A total of 803 cells were discarded in this step, as they were unassigned to any of the 30 clusters or there was no difference in the median expression of *Slc17a6* and *Slc32a1*. Furthermore, 17 cells were unassigned to non-neuronal clusters, 80 cells were unassigned to glutamatergic clusters and 71 cells were unassigned to GABAergic clusters. Marker genes were identified using area under a receiver operating characteristic curve (AUROC) analysis. All genes that are greater than twofold expressed in the cluster compared with the rest of the population were analyzed using AUROC. Genes that had greater than 85% classification score were defined as markers specific to the cell type. Genes differentially expressed in a given cluster were computed using edgeR. Expression of marker genes in each cluster were represented as violin plots. Violin plots were rendered using the ggplot2 package in R. They represent the distribution of log-transformed normalized gene expression (gene UMIs/total cell UMIs) in each cluster. The maximum expression for each of violin plot was set to 5. Marker genes were used for provisional cluster names that included one to three markers. A cluster name denoted by a single marker indicates a gene that is selectively and robustly expressed by a single cluster and is sufficient to define that cluster. The addition of a second marker indicates a secondary identifier that is also strongly, although not necessarily uniquely, expressed in the cluster. *Gad1* was added to the four LHA$^{\text{Glut}}$ clusters that robustly expressed it, despite being classified as glutamatergic. Finally, we found that although *Pmch* and *Hcrt* expression was sufficient to identify LHA$^{\text{Glut}}$ clusters 1 and 6, respectively, they were unique in also being expressed at low, but consistent, levels in every other LHA$^{\text{Glut}}$ and LHA$^{\text{GABA}}$ cluster. This is likely explained by ambient mRNA released from damaged neurons during dissociation.

FACS analysis.

For sc-qPCR experiments on FACS-sorted single cells, hypothalamic brain slices were obtained from male juvenile mutant mice (P25–32). FACS for *Pmch*-Cre;EYFP ($n = 3$ mice), *Nts*-Cre;EYFP ($n = 3$ mice) and *Sst*-IRES-Cre;EYFP ($n = 3$ mice) was performed in two batches. FACS for *Lepr*-Cre;EYFP ($n = 2$ mice) was done in a single batch, and FACS for Ox-EGFP ($n = 11$ mice) was performed in four batches. Data from each batch were pooled. FACS was carried out as previously described[8]. Briefly, EGFP+ or EYFP+ neurons were sorted on a BD FACSAria II Cell Sorter (BD Biosciences; University of Connecticut Flow Cytometry Facility) equipped with a sapphire 488 nm excitation laser (Coherent) using BD FACSDiva software. A 10 K threshold was applied to filter debris from the media. Cells were selected based on scatter (SSC-A versus FSC-A) and for singlets based on side-scatter (SSC-W versus SSC-H) and forward-scatter (FSC-W versus FSC-H), then gated on the presence of EGFP or EYFP fluorescence (PE-A versus GFP-A). Cells were then sorted in single-cell precision mode into a sterile 96-well plate containing 2.5 μl lysis buffer (0.5% NP-40, 1 U μl^{-1} RNAsin+ (Promega), 0.25× pooled Taqman assays), snap-frozen on dry ice and stored at −80 °C until processing for sc-qPCR.

sc-qPCR.

Plates of FACS-sorted cells were thawed, and a combined lysis and denaturation step was performed by incubation at 70 °C for 4 min, 4 °C for 5 min. Reverse transcription (RT) master mix (2.5 μl) was then added to each well (1 μl 5× RT Buffer (Promega), 0.6 μl 35 mM $MgCl_2$, 0.25 μl Moloney Murine Leukemia Virus (MMLV) (Promega), 0.1 μl 25 mM dNTPs, 0.5 μl H_2O) and incubated at 37 °C for 2 min, 42 °C for 1 min and 50 °C for 1 s for 40 cycles, then 85 °C for 5 min, and 4 °C hold. Following RT, cDNA was pre-amplified by adding 2 μl of cDNA from the RT plate to 8 μl of preamp master mix (5 μl TaKaRa premix Taq polymerase (Clontech), 2.5 μl 0.25× Taqman pool, 0.5 μl H_2O) and thermocycled at 95 °C for 3 min, 55 °C for 2 min, 72 °C for 2 min, then 95 °C for 15 s, 60 °C for 2 min, 72 °C for 2 min for 16 cycles, and 4 °C hold. Amplified cDNA was then diluted 1:50 in nuclease-free H_2O and this material was used for qPCR against a curated panel of 30 TaqMan Gene Expression Assays (Supplementary Table 2) on 48.48 dynamic arrays using a Biomark HD system (Fluidigm).

qPCR data analysis.

Raw cycle threshold (Ct) values were obtained from the Fluidigm Biomark software and inverted (35-Ct) to generate a $\log_2$-based scale for gene expression analysis. To eliminate cells with low or no cDNA yield, we filtered our dataset to include only cells within the 95% confidence interval for *Gapdh* expression after removing cells absent for the defining transcript. Hierarchical clustering was performed using Ward's method with complete linkage[59]. All statistical analyses were performed using R v.3.1.0 (The R Project for Statistical Computing; www.r-project.org).

FISH.

FISH was carried out as previously described[8]. Briefly, to prepare tissue sections for FISH, male juvenile wild-type C57BL/6 mice (P25–38) were anesthetized with isoflurane,

decapitated and brains were dissected out into ice-cold sucrose. Brains were rapidly frozen on dry ice, embedded in OCT compound and cryosectioned at a thickness of 14 μm onto SuperFrost Plus microscope slides. Sections were fixed with 4% paraformaldehyde (PFA) at 4 °C for 15 min, and then dehydrated in 50, 70 and 100% ethanol. RNAscope 2.5 Assay (Advanced Cell Diagnostics) was used for all FISH experiments according to the manufacturer's protocols[60]. All RNAscope FISH probes were designed and validated by Advanced Cell Diagnostics. ISH images from the Allen Brain Institute were acquired from the publicly available resource the Allen Mouse Brain Atlas (www.mouse.brain-map.org/)[9] and used in Supplementary Figs. 4 and 5. Single discriminatory markers were shown for each neuronal cluster, with several ISH images (for example, *Sst* and *Trh*) being repeated, and some images being unavailable (for example, *Atp1a2*). ISH images were acquired with minor contrast adjustments as needed, and converted to grayscale, to maintain image consistency.

FISH combined with immunohistochemistry.

To prepare sections for FISH and immunohistochemistry (IHC), male juvenile mice (P30–38) injected with 0.5% CTb in the lateral septum were anesthetized with ketamine and xylazine and perfused with 0.125 M saline then 4% PFA. Brains were post-fixed overnight and rapidly frozen on dry ice, embedded in OCT compound and cryosectioned at a thickness of 20 μm and mounted onto SuperFrost Plus microscope slides. RNAscope 2.5 Assay (Advanced Cell Diagnostics) was used for all FISH experiments according to the manufacturer's protocols[60]. All RNAscope FISH probes were designed and validated by Advanced Cell Diagnostics. Following the FISH protocol, sections were blocked for 10 min in 10% donkey normal serum (DNS) in phosphate-buffered saline (PBS) solution supplemented with 0.2% Tween-20 (PBST), then incubated for 1 h with goat anti-CTb (1:2,000; List Biological Laboratories, no. 703, lot no. 7032A10). Sections were then washed with PBS (two times for 2 min each), then incubated for 30 min with donkey anti-goat Alexa Fluor 594 (1:500; Abcam, no. ab150132). Sections were then washed with RNAscope 1× wash buffer (two times for 2 min each), then mounted using ProLong Gold Antifade mountant with DAPI (Thermo Fisher Scientific, no. P36935).

Imaging and image quantification of FISH data.

Quantification of FISH data from confocal images was carried out as previously described[8]. Confocal images of FISH and combined FISH and IHC experiments were obtained using a Leica TSC Sp8, and confocal image files (.lif) containing image stacks were loaded into ImageJ (v.2.0.0, NIH) and processed to analyze the percentage co-localization of various mRNA transcripts. Cells were marked and categorized using the ImageJ Cell Counter plugin. Expression was denoted as binary yes/no dependent on the fulfillment of a defined criteria; the presence of at least five punctate fluorescent dots accompanying a nucleus labeled by 4′,6-diamidino-2-phenylindole (DAPI) (Vector Laboratories). Cells that were double-labeled in the tetramethylrhodamine, cyanine 5 and/or FITC (fluorescein isothiocyanate) channels were identified as cells exhibiting co-localization. This process was repeated for multiple.lif files for each FISH experiment, and pie charts were used to display percentage co-localization, whereby the *n* values describe the total number of cells analyzed.

Brain slice electrophysiology.

Male and female *Sst*-Cre;EYFP mice (4 males and 6 females, 1–2 months old) were anesthetized using inhaled isoflurane and injected intraperitoneally with ketamine and xylazine. Transcardial perfusion was performed with 20 ml of ice-cold sucrose solution containing the following components (in mM): 87 NaCl, 75 sucrose, 25 glucose, 25 NaHCO$_3$, 7.5 MgCl$_2$, 2.5 KCl, 1.25 NaH$_2$PO$_4$, 0.5 CaCl$_2$ and 5 ascorbic acid. After perfusion, mice were decapitated and brains carefully dissected. Coronal slices (225 μm thick) capturing the LHA were collected using a vibrating microtome (7000smz-2, Campden Instruments) and incubated at 34 °C for 45 min in artificial CSF (ACSF) containing the following components (in mM): 125 NaCl, 25 NaHCO$_3$, 11 glucose, 2.5 KCl, 1.25 NaH$_2$PO$_4$, 1 MgCl$_2$ and 2 CaCl$_2$ (~305 mOsm per liter). Slices were then maintained at room temperature for at least 30 min before recording. Sucrose and ACSF solutions were continuously bubbled with 95% O$_2$/5% CO$_2$.

Slices were placed in the recording chamber of an upright Olympus BX51 microscope (Olympus America) and continuously superfused with bubbling ACSF containing blockers of fast synaptic transmission (1 mM kynurenic acid and 100 μM picrotoxin), at physiological temperature (34–35 °C). Cells in the perifonical LHA and tuberal region were visualized using infrared differential interference contrast. *Sst*$^+$ neurons were identified based on EYFP expression using epifluorescence illumination. Whole-cell current-clamp and voltage-clamp recordings were obtained using a Multiclamp 700B amplifier and pClamp10 acquisition software (Molecular Devices). Recording pipettes were pulled with a Flaming/Brown micropipette puller (P-1000, Sutter Instruments) and filled with an internal solution containing the following components (in mM): 130 K-gluconate, 10 HEPES, 0.1 EGTA, 10 NaCl, 2 MgCl$_2$, 10 phosphocreatine di(tris), 4 Mg-ATP and 0.3 Na-GTP (290 mOsm per liter), pH 7.2. Access resistance values >20 MOhm were excluded from the analysis. In total, we recorded and analyzed data from 40 perifonical *Sst*$^+$ neurons (4 males, 4 females) and 19 tuberal *Sst*$^+$ neurons (4 males, 4 females).

Analysis of electrophysiological data.

Data were analyzed using ClampFit 10.4 (Molecular Devices) and custom scripts written in MATLAB R2016b (MathWorks). In current-clamp experiments, cells were initially recorded in gap-free mode in an undisturbed state to obtain the resting membrane potential (RMP) if silent, or the firing rate (if active). Cells were then subjected to a hyperpolarizing step of 20 pA for 1 s to obtain the repolarization latency and spike ratio values. Repolarization latency was defined as the time to the first spike after the release of the current injection. The spike ratio was quantified as the ratio of spikes before and after the hyperpolarizing step. In this set of protocols, silent cells were injected with current to fire slightly above threshold. To obtain electrical properties related to the action potential (AP), cells were held at −80 mV and underwent depolarizing steps of 5 pA for 1 s. Rheobase current was defined at the first evoked AP and related properties were extracted from this single AP. The AP threshold was defined as where the first derivative of the voltage (dV/dt) was 2% of the maximum value. Relative to the amplitude of AP threshold, AP amplitude and afterhyperpolarization amplitude were determined. Additionally, at the midpoint between AP peak and AP threshold, the AP half-width was extracted. Both decay and rise times are calculated on the

basis of 10–90% of the absolute AP threshold and AP peak. In voltage-clamp recordings, passive properties were obtained using a 100 ms hyperpolarizing step of −5 mV. Traces were averaged for each cell, and the input resistance was determined using the change in current 50 ms before the step and the last 50 ms during the step. Membrane capacitance was calculated by subtracting the holding current from the averaged trace and integrating the area under the transient. Membrane potential values were corrected for the liquid junction potential, which was calculated as 10.2 mV using pClamp10. Statistical analysis between electrical properties were performed using unpaired two-sample Wilcoxon rank sum test, and statistical significance is indicated as follows: $*P < 0.05$ and $**P < 0.01$.

Biocytin staining and imaging.

A selection of Sst^+ neurons in the perifornical and tuberal regions were filled with internal solution containing 0.1% biocytin (Sigma-Aldrich). In whole-cell configuration, cells were filled for at least 5 min. The pipette was gently removed from the cell to preserve morphology and EYFP expression of the cell. Slices were then fixed in 4% PFA (in PBS) for 30 min and stored in 0.5% Triton X-100 plus 5% DNS (in PBS) overnight at 4 °C. For staining, slices were incubated with streptavidin conjugated to Alexa Fluor 594 (1:500; Thermo Fisher Scientific, no. S11227) for 2 h at room temperature. After four repeated washes of 10 min in 0.5% Triton X-100 (in PBS), slices were mounted onto slides with Vectashield with DAPI.

Stereotactic injection and histology.

For anterograde projection experiments, male P21–32 *Vgat*-Cre, *Vglut2*-Cre or *Sst*-Cre mice were bilaterally injected with 25–50 nl of AAV2-EF1α-DIO-hChR2(H134R)-EYFP (UNC Viral Core, Deisseroth Lab) into the LHA (anteroposterior (AP): −1.5, mediolateral (ML): ±1.1, dorsoventral (DV): −5.3 mm), and allowed to incubate for 4–5 weeks. *Sst*-Cre mice were injected with 25 nl, while *Vgat*-Cre and *Vglut2*-Cre mice were injected with 50 nl. For retrograde projection experiments, male C57BL/6 P30–45 mice were bilaterally injected with 50–100 nl of 0.5% CTb (List Biological Laboratories, no. 104, lot no. 10433A1, diluted in sterile saline) into the dLS (AP: +0.5, ML: ±0.35, DV: −3.0 mm), and allowed to incubate for 1 week before FISH and IHC experiments. For chemogenetic behavioral experiments, male P30–37 *Sst*-Cre mice were bilaterally injected with 25 nl of AAV8.2-hEF1α-DIO-hM3Dq-mCherry-WPRE (MGH Viral Core, no. AAV-RN4) or AAV8.2-hEF1α-DIO-mCherry-WPRE control virus (MGH Viral Core, no. AAV-RN12) into the LHA, and allowed to incubate for 3–4 weeks before behavioral tests. For histology, mice were killed with ketamine and xylazine and transcardially perfused with 10 ml 0.125 M saline, followed by 40 ml 4% PFA in 1× PBS (pH 7.4), and brains were dissected and post-fixed in 4% PFA for 24 h, followed by cyroprotection in 30% sucrose for 48 h. Brains were then flash frozen with cold isopentane and stored at −80 °C. Frozen brains were cut into 40–50 μm thick coronal sections containing the LHA or dLS injection sites on a cryostat (Leica CM 3050s). For c-Fos IHC staining, 40 μm coronal sections were incubated with rabbit-anti-c-Fos (1:2,000; Cell Signaling, no. 2250) overnight at room temperature, then with secondary antibody donkey-anti-rabbit Alexa Fluor 488 (1:500; Abcam, no. ab150073) for 2 h at room temperature. Sections were washed in 1× PBS before being mounted onto slides and coverslipped with Vectashield hardset mounting media with DAPI (Vector Labs). Injection

sites were imaged at ×10 magnification on a fluorescence microscope (Zeiss Axio Zoom V16 Stereo Zoom or Keyence BZ-X700). Images were processed with ImageJ, Adobe Photoshop CS and Adobe Illustrator CC. Based on post hoc histological evaluation of the injection site, mice were excluded from the behavioral analysis if bilateral injections were off-target, found to be unilateral and/or significantly smaller than anticipated.

Behavioral assay with video tracking.

Sst-Cre mice were bilaterally injected (25 nl each side) with AAV8.2-EF1α-DIO-hM3Dq-mCherry ($n = 4$) or AAV8.2-EF1α-DIO-mCherry ($n = 6$) and allowed to incubate for 3–4 weeks before behavioral tests. Mice were habituated to behavioral chambers for 24 h before behavioral tests. In the behavioral chambers with both top- and side-mounted cameras (Noldus PhenoTyper homecage; Noldus Information Technology), mice had access to food pellets (on the floor), a water spout, a cotton fiber bedding nestlet, a 3-inch manzanita wood gnawing stick (Bio-Serv) and 10 wooden sticks (uniform segments of sterile wooden cotton applicator sticks). On the day of behavioral testing, food pellets were replaced with fresh food and the mice were then video recorded for a 3 h pre-injection habituation period. Mice were then removed from the cage, injected intraperitoneally with 1 mg per kg CNO, placed back in the cage and a 2 h post-injection period was recorded. A comparison was made between a 1 h pre-injection period immediately before intraperitoneal injection and a 1 h post-injection period measured 15 min following intraperitoneal injection. All experiments took place early in the light/inactive period (8:00–13:00). Videos were acquired using Noldus Ethovision (Noldus Information Technology), from the top and side views simultaneously. Tracking data for nose-point and center-point from the top view were generated using Noldus Ethovision 13 software. Side view videos from pre-injection and post-injection segments were manually scored for the following ten independent behaviors (modified from a previous study[61]): rearing, gnawing, resting, walking, shredding, eating, drinking, digging, grooming and nest activity (defined as indeterminate mouse activity engaged in within the nest, being slightly obscured by the nest). Behaviors that persisted for 3 s or more were scored. Video scoring was performed post hoc by a blinded scorer using Noldus Ethovision 13 software. Statistical differences were analyzed using unpaired two-sample Wilcoxon rank sum test performed in R (The R Project for Statistical Computing; www.r-project.org).

Statistics and reproducibility.

No statistical methods were used to predetermine sample sizes, but our sample sizes were similar to those reported in previous publications[62–64]. For behavioral and electrophysiology experiments, we used unpaired, two-sample Wilcoxon rank sum test and report mean values with error bars representing standard errors of the mean. Individual data points are shown and not assumed to be normally distributed, nor was normality formally tested. Mice were arbitrarily assigned for scRNA-seq, sc-qPCR, FISH, electrophysiology, stereotaxic surgery and behavioral experiments, and analyses were performed accordingly. For FISH, sc-qPCR and electrophysiology experiments, data collection and analyses were not performed blinded to the experimental conditions. For behavioral experiments, data collection was not blinded to the experimental conditions, but analysis was performed in a blinded manner.

Reporting Summary.

Further information on research design is available in the Nature Research Reporting Summary linked to this article.

Code availability

No specific custom code was developed for this analysis. The analysis routine for the single-cell data is defined in the scRNA-seq analysis section and further details, if needed, provided upon request. Interactive analysis was done using the CellView RShiny web application[65].

Data availability

All data that support the findings of this study are available as raw data in GEO at GSE125065.

Supplementary Material

Refer to Web version on PubMed Central for supplementary material.

Acknowledgements

References

1. Brown JA, Woodworth HL & Leinninger GM To ingest or rest? Specialized roles of lateral hypothalamic area neurons in coordinating energy balance. Front. Syst. Neurosci 9, 9 (2015). [PubMed: 25741247]

2. Bonnavion P, Mickelsen LE, Fujita A, de Lecea L & Jackson AC Hubs and spokes of the lateral hypothalamus: cell types, circuits and behaviour. J. Physiol. (Lond.) 594, 6443–6462 (2016). [PubMed: 27302606]

3. Stuber GD & Wise RA Lateral hypothalamic circuits for feeding and reward. Nat. Neurosci 19, 198–205 (2016). [PubMed: 26814589]

4. Swanson LW, Sanchez-Watts G & Watts AG Comparison of melanin-concentrating hormone and hypocretin/orexin mRNA expression patterns in a new parceling scheme of the lateral hypothalamic zone. Neurosci. Lett 387, 80–84 (2005). [PubMed: 16084021]

5. Sakurai T The role of orexin in motivated behaviours. Nat. Rev. Neurosci 15, 719–731 (2014). [PubMed: 25301357]

6. Diniz GB & Bittencourt JC The melanin-concentrating hormone as an integrative peptide driving motivated behaviors. Front. Syst. Neurosci 11, 32 (2017). [PubMed: 28611599]

7. Herrera CG, Ponomarenko A, Korotkova T, Burdakov D & Adamantidis A Sleep & metabolism: the multitasking ability of lateral hypothalamic inhibitory circuitries. Front. Neuroendocrinol 44, 27–34 (2017). [PubMed: 27884682]

8. Mickelsen LE et al. Neurochemical heterogeneity among lateral hypothalamic hypocretin/orexin and melanin-concentrating hormone neurons identified through single cell gene expression analysis. eNeuro 4, 1–24 (2017).

9. Lein ES et al. Genome-wide atlas of gene expression in the adult mouse brain. Nature 445, 168–176 (2007). [PubMed: 17151600]

10. Marston OJ, Hurst P, Evans ML, Burdakov DI & Heisler LK Neuropeptide Y cells represent a distinct glucose-sensing population in the lateral hypothalamus. Endocrinology 152, 4046–4052 (2011). [PubMed: 21914773]

11. Motoike T et al. Transient expression of neuropeptide W in postnatal mouse hypothalamus—a putative regulator of energy homeostasis. Neuroscience 301, 323–337 (2015). [PubMed: 26073698]

12. Horjales-Araujo E, Hellysaz A & Broberger C Lateral hypothalamic thyrotropin-releasing hormone neurons: distribution and relationship to histochemically defined cell populations in the rat. Neuroscience 277, 87–102 (2014). [PubMed: 24993479]

13. Shimogori T et al. A genomic atlas of mouse hypothalamic development. Nat. Neurosci 13, 767–775 (2010). [PubMed: 20436479]

14. Liu K et al. Lhx6-positive GABA-releasing neurons of the zona incerta promote sleep. Nature 548, 582–587 (2017). [PubMed: 28847002]

15. Dalal J et al. Translational profiling of hypocretin neurons identifies candidate molecules for sleep regulation. Genes Dev 27, 565–578 (2013). [PubMed: 23431030]

16. Broberger C Hypothalamic cocaine- and amphetamine-regulated transcript (CART) neurons: histochemical relationship to thyrotropin-releasing hormone, melanin-concentrating hormone, orexin/hypocretin and neuropeptide Y. Brain Res 848, 101–113 (1999). [PubMed: 10612702]

17. Elias CF et al. Characterization of CART neurons in the rat and human hypothalamus. J. Comp. Neurol 432, 1–19 (2001). [PubMed: 11241374]

18. Brischoux F, Fellmann D & Risold PY Ontogenetic development of the diencephalic MCH neurons: a hypothalamic 'MCH area' hypothesis. Eur. J. Neurosci 13, 1733–1744 (2001). [PubMed: 11359525]

19. Cvetkovic V et al. Characterization of subpopulations of neurons producing melanin-concentrating hormone in the rat ventral diencephalon. J. Neurochem 91, 911–919 (2004). [PubMed: 15525345]

20. Leinninger GM et al. Leptin action via neurotensin neurons controls orexin, the mesolimbic dopamine system and energy balance. Cell Metab 14, 313–323 (2011). [PubMed: 21907138]

21. Leinninger GM et al. Leptin acts via leptin receptor-expressing lateral hypothalamic neurons to modulate the mesolimbic dopamine system and suppress feeding. Cell Metab 10, 89–98 (2009). [PubMed: 19656487]

22. Cui H et al. Neuroanatomy of melanocortin-4 receptor pathway in the lateral hypothalamic area. J. Comp. Neurol 520, 4168–4183 (2012). [PubMed: 22605619]

23. Laque A et al. Leptin receptor neurons in the mouse hypothalamus are colocalized with the neuropeptide galanin and mediate anorexigenic leptin action. Am. J. Physiol. Endocrinol. Metab 304, E999–E1011 (2013). [PubMed: 23482448]

24. Romanov RA et al. Molecular interrogation of hypothalamic organization reveals distinct dopamine neuronal subtypes. Nat. Neurosci 20, 176–188 (2017). [PubMed: 27991900]

25. Morales-Delgado N et al. Topography of somatostatin gene expression relative to molecular progenitor domains during ontogeny of the mouse hypothalamus. Front. Neuroanat 5, 10 (2011). [PubMed: 21441981]

26. Nieh EHH et al. Decoding neural circuits that control compulsive sucrose seeking. Cell 160, 528–541 (2015). [PubMed: 25635460]

27. Nieh EH et al. Inhibitory input from the lateral hypothalamus to the ventral tegmental area disinhibits dopamine neurons and promotes behavioral activation. Neuron 90, 1286–1298 (2016). [PubMed: 27238864]

28. Herrera CG et al. Hypothalamic feedforward inhibition of thalamocortical network controls arousal and consciousness. Nat. Neurosci 19, 290–298 (2016). [PubMed: 26691833]

29. Jennings JHH et al. Visualizing hypothalamic network dynamics for appetitive and consummatory behaviors. Cell 160, 516–527 (2015). [PubMed: 25635459]

30. Barbano MF, Wang H-L, Morales M & Wise RA Feeding and reward are differentially induced by activating GABAergic lateral hypothalamic projections to VTA. J. Neurosci 36, 2975–2985 (2016). [PubMed: 26961951]

31. Navarro M et al. Lateral hypothalamus GABAergic neurons modulate consummatory behaviors regardless of the caloric content or biological relevance of the consumed stimuli. Neuropsychopharmacology 41, 1505–1512 (2016). [PubMed: 26442599]

32. Venner A, Anaclet C, Broadhurst RY, Saper CB & Fuller PM A novel population of wake-promoting GABAergic neurons in the ventral lateral hypothalamus. Curr. Biol 26, 2137–2143 (2016). [PubMed: 27426511]

33. Kosse C, Schöne C, Bracey E & Burdakov D Orexin-driven GAD65 network of the lateral hypothalamus sets physical activity in mice. Proc. Natl Acad. Sci. USA 114, 4525–4530 (2017). [PubMed: 28396414]

34. Schöne C, Apergis-Schoute J, Sakurai T, Adamantidis A & Burdakov D Coreleased orexin and glutamate evoke nonredundant spike outputs and computations in histamine neurons. Cell Rep 7, 697–704 (2014). [PubMed: 24767990]

35. Wallace ML et al. Genetically distinct parallel pathways in the entopeduncular nucleus for limbic and sensorimotor output of the basal ganglia. Neuron 94, 138–152 (2017). [PubMed: 28384468]

36. Li Y et al. Hypothalamic circuits for predation and evasion. Neuron 97, 911–924 (2018). [PubMed: 29398361]

37. Karnani MM, Szabó G, Erdélyi F & Burdakov D Lateral hypothalamic GAD65 neurons are spontaneously firing and distinct from orexin- and melanin-concentrating hormone neurons. J. Physiol. (Lond.) 591, 933–953 (2013). [PubMed: 23184514]

38. Hassani OK, Henny P, Lee MG & Jones BE GABAergic neurons intermingled with orexin and MCH neurons in the lateral hypothalamus discharge maximally during sleep. Eur. J. Neurosci 32, 448–457 (2010). [PubMed: 20597977]

39. Bonnavion P, Jackson AC, Carter ME & de Lecea L Antagonistic interplay between hypocretin and leptin in the lateral hypothalamus regulates stress responses. Nat. Commun 6, 6266 (2015). [PubMed: 25695914]

40. Patterson CM et al. Ventral tegmental area neurotensin signaling links the lateral hypothalamus to locomotor activity and striatal dopamine efflux in male mice. Endocrinology 156, 1692–1700 (2015). [PubMed: 25734363]

41. Woodworth HL et al. Lateral hypothalamic neurotensin neurons orchestrate dual weight loss behaviors via distinct mechanisms. Cell Rep 21, 3116–3128 (2017). [PubMed: 29241540]

42. Qualls-Creekmore E et al. Galanin-expressing GABA neurons in the lateral hypothalamus modulate food reward and non-compulsive locomotion. J. Neurosci 37, 6053–6065 (2017). [PubMed: 28539422]

43. Jennings JH, Rizzi G, Stamatakis AM, Ung RL & Stuber GD The inhibitory circuit architecture of the lateral hypothalamus orchestrates feeding. Science 341, 1517–1521 (2013). [PubMed: 24072922]

44. Stamatakis AM et al. Lateral hypothalamic area glutamatergic neurons and their projections to the lateral habenula regulate feeding and reward. J. Neurosci 36, 302–311 (2016). [PubMed: 26758824]

45. Lechan RM & Fekete C The TRH neuron: a hypothalamic integrator of energy metabolism. Prog. Brain Res 153, 209–235 (2006). [PubMed: 16876577]

46. Han W et al. Integrated control of predatory hunting by the central nucleus of the amygdala. Cell 168, 311–324 (2017). [PubMed: 28086095]

47. Carus-Cadavieco M et al. Gamma oscillations organize top-down signalling to hypothalamus and enable food seeking. Nature 542, 232–236 (2017). [PubMed: 28146472]

48. Luo SX et al. Regulation of feeding by somatostatin neurons in the tuberal nucleus. Science 361, 76–81 (2018). [PubMed: 29976824]

49. Campbell JN et al. A molecular census of arcuate hypothalamus and median eminence cell types. Nat. Neurosci 20, 484–496 (2017). [PubMed: 28166221]

50. Chen R, Wu X, Jiang L & Zhang Y Single-cell RNA-Seq reveals hypothalamic cell diversity. Cell Rep 18, 3227–3241 (2017). [PubMed: 28355573]

51. Madisen L et al. A robust and high-throughput Cre reporting and characterization system for the whole mouse brain. Nat. Neurosci 13, 133–140 (2010). [PubMed: 20023653]

52. Kong D et al. Glucose stimulation of hypothalamic MCH neurons involves K(ATP) channels, is modulated by UCP2, and regulates peripheral glucose homeostasis. Cell Metab 12, 545–552 (2010). [PubMed: 21035764]

53. Taniguchi H et al. A resource of Cre driver lines for genetic targeting of GABAergic neurons in cerebral cortex. Neuron 71, 995–1013 (2011). [PubMed: 21943598]

54. Leshan RL, Björnholm M, Münzberg H & Myers MG Jr. Leptin receptor signalingand action in the central nervous system. Obesity (Silver Spring) 14 Suppl 5, 208S–212S (2006). [PubMed: 17021368]

55. Sakurai T et al. Structure and function of human prepro-orexin gene. J. Biol. Chem 274, 17771–17776 (1999). [PubMed: 10364220]

56. Yamanaka A et al. Hypothalamic orexin neurons regulate arousal according to energy balance in mice. Neuron 38, 701–713 (2003). [PubMed: 12797956]

57. Vong L et al. Leptin action on GABAergic neurons prevents obesity and reduces inhibitory tone to POMC neurons. Neuron 71, 142–154 (2011). [PubMed: 21745644]

58. Paxinos G & Franklin KBJ The Mouse Brain in Stereotaxic Coordinates (Academic, Amsterdam, 2012).

59. Ward JH Hierarchical grouping to optimize an objective function. J. Am. Stat. Assoc 58, 236–244 (1963).

60. Wang F et al. RNAscope: a novel in situ RNA analysis platform for formalin-fixed, paraffin-embedded tissues. J. Mol. Diagn 14, 22–29 (2012). [PubMed: 22166544]

61. Füzesi T, Daviu N, Wamsteeker Cusulin JI, Bonin RP & Bains JS Hypothalamic CRH neurons orchestrate complex behaviours after stress. Nat. Commun 7, 11937 (2016). [PubMed: 27306314]

62. Rheaume BA et al. Single cell transcriptome profiling of retinal ganglion cells identifies cellular subtypes. Nat. Commun 9, 2759 (2018). [PubMed: 30018341]

63. Harris KD et al. Classes and continua of hippocampal CA1 inhibitory neurons revealed by single-cell transcriptomics. PLoS Biol 16, e2006387 (2018). [PubMed: 29912866]

64. Gupta I et al. Single-cell isoform RNA sequencing characterizes isoforms in thousands of cerebellar cells. Nat. Biotechnol 36, 1197–1202 (2018).

65. Bolisetty MT, Stitzel ML & Robson P CellView: interactive exploration of high dimensional single cell RNA-seq data. Preprint at 10.1101/123810 (2017).

Author Manuscript

Author Manuscript

Author Manuscript

Author Manuscript
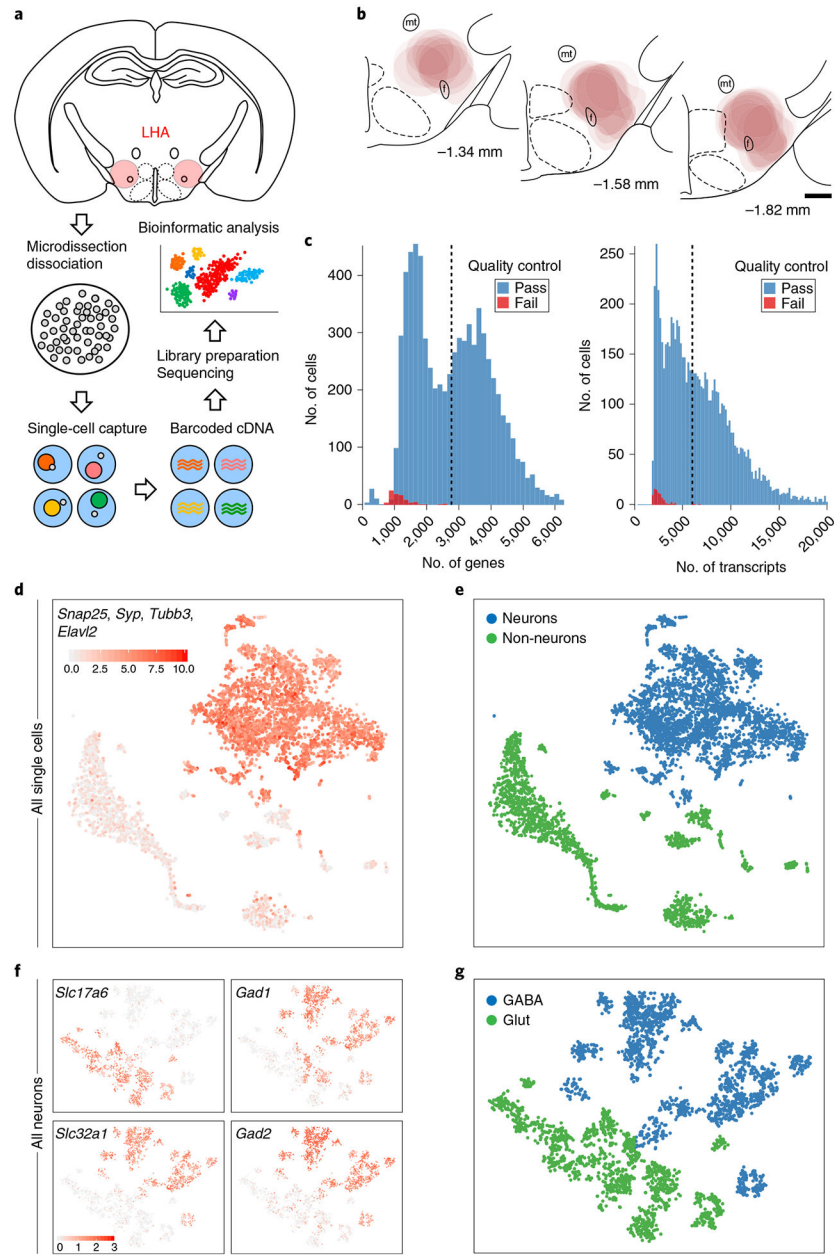
Fig. 1 |. scRNA-seq of LHA cell populations.
a, Schematic representation of the workflow for LHA microdissection, single-cell isolation, cDNA library preparation, sequencing and clustering. **b**, Location of LHA microdissections from male and female C57BL/6 mice, mapped onto coronal mouse brain atlas images corresponding to distances from bregma of −1.34, −1.58 and −1.82 mm. mt, mammillothalamic tract; f, fornix. Scale bar, 500 μm. **c**, Histograms of genes and transcripts (UMIs) detected in 7,129 single cells. **d**, Sum of normalized expression of pan-neuronal markers in each cell shown on a t-SNE plot after the first iteration of unsupervised clustering ($n = 6,944$ cells). **e**, Cells were classified using a Gaussian mixture model as neurons or non-neurons based on the combined expression of pan-neuronal markers ($n = 6,944$ cells). **f**, Normalized expression of *Slc17a6*, *Slc32a1*, *Gad1* and *Gad2* in each cell shown on a t-SNE
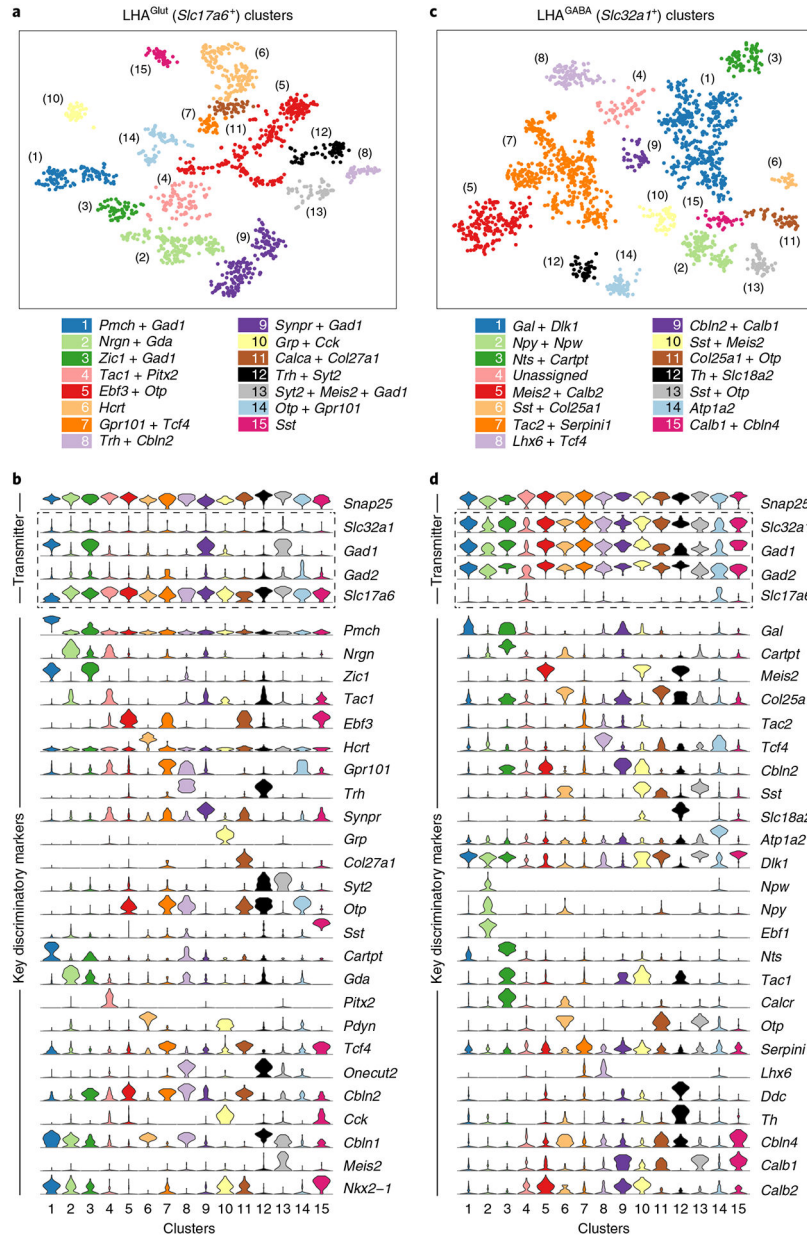
plot after the second iteration of unsupervised clustering of neuronal cells ($n = 3,589$ cells in each panel). **g**, Neurons were classified as either GABAergic or glutamatergic based on the expression of *Slc32a1* and *Slc17a6*, respectively ($n = 3,589$ cells).

Fig. 2 |. Classification of LHA^Glut and LHA^GABA neuronal cell types in the LHA.
a, Unsupervised clustering of LHA^Glut neuronal cell types represented in a t-SNE plot ($n =$ 1,537 cells). Cell-type clusters are color coded, with classifications below the plot. **b**, Violin plot, representing the distribution of log-transformed normalized gene expression (gene UMIs/total cell UMIs) in each cluster, of the pan-neuronal marker *Snap25*, neurotransmitter components (*Slc32a1*, *Gad1*, *Gad2* and *Slc17a6*) (upper) and discriminatory markers (lower) for LHA^Glut neuronal cell types ($n =$ 1,537 cells). **c**, Unsupervised clustering of LHA^GABA neuronal cell types represented in a t-SNE plot ($n =$ 1,900 cells). Different cell-type clusters are color coded, with classifications below the plot. **d**, Violin plot showing normalized expression of neuronal, neurotransmitter (upper) and discriminatory markers (lower) for
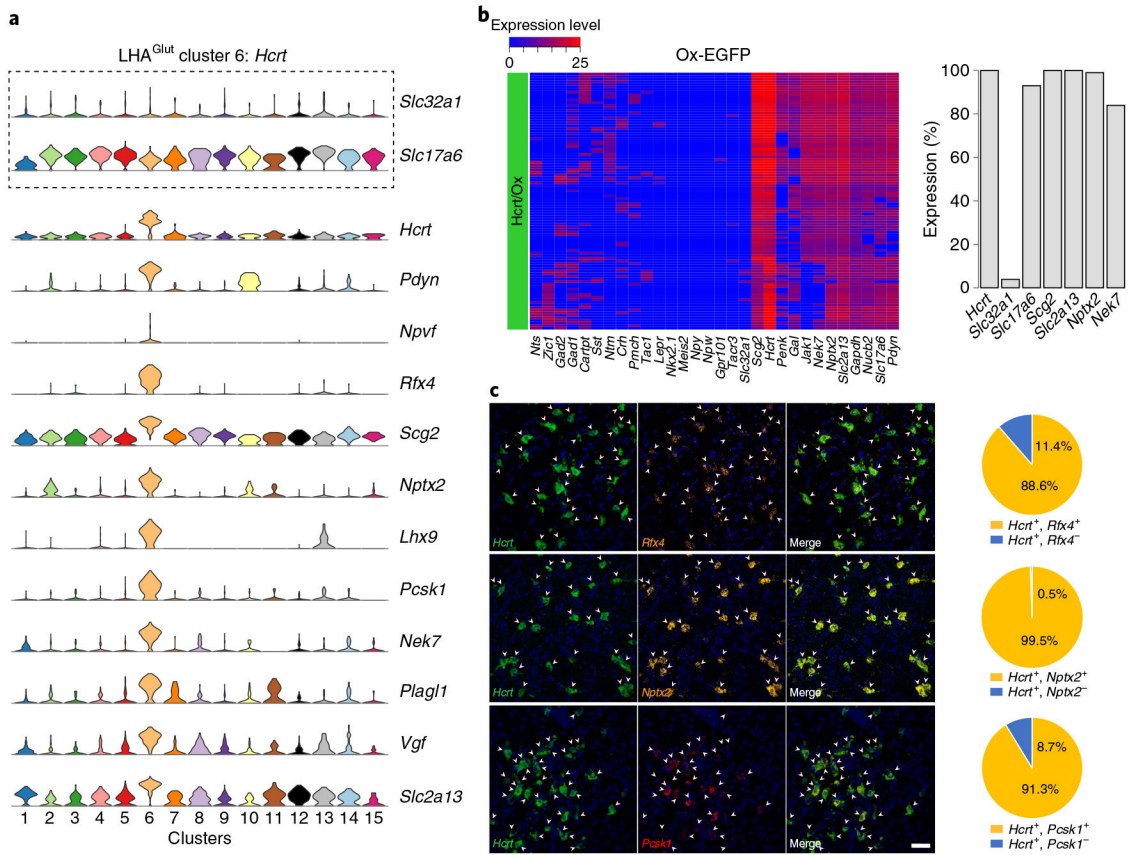
LHA$^{\text{GABA}}$ neuronal cell types ($n = 1{,}900$ cells). Total number of cells per cluster, mean genes per cell and mean UMIs per cell are provided in Supplementary Table 1.

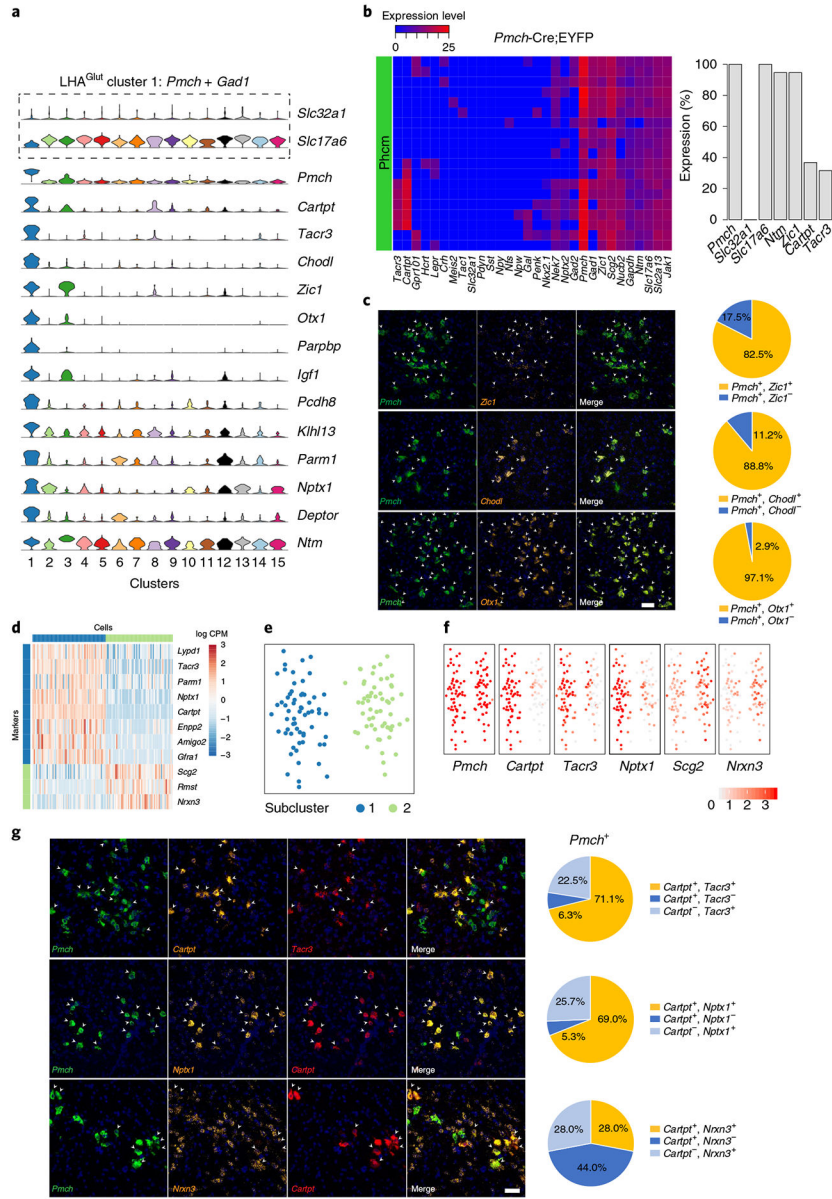**Fig. 3 |. Validation of discriminatory marker expression in LHA^{Glut} *Hcrt*-expressing neurons.**
a, Violin plot, representing the distribution of log-transformed normalized gene expression (gene UMIs/total cell UMIs), of *Slc32a1*, *Slc17a6* and discriminatory markers of LHA^{Glut} cluster 6 (*Hcrt*) neurons ($n = 162$ cells). Total number of cells, mean genes per cell and mean UMIs per cell are provided in Supplementary Table 1. **b**, Left: heatmap of 100 single *Hcrt*$^+$ neurons and their expression of 30 genes by qPCR ($n = 11$ mice). Heatmap colors depict expression levels on a $\log_2$ scale from low (blue) to high (red). Right: bar graph measuring percentage expression for seven genes in single *Hcrt*$^+$ neurons. **c**, Confocal micrographs ($\times$40) of coronal sections of wild-type mice and corresponding pie charts representing co-expression of mRNA for *Hcrt* and *Rfx4* ($n = 675$ cells, 4 mice; upper), *Hcrt* and *Nptx2* ($n = 203$ cells, 4 mice; middle), and *Hcrt* and *Pcsk1* ($n = 675$ cells, 3 mice; lower). All sections were counterstained with DAPI (blue). White arrowheads indicate co-localization. Scale bar (applicable to all micrographs), 50 μm.

Fig. 4 |. Validation of discriminatory marker expression in LHA^Glut *Pmch*-expressing neurons and subpopulations.
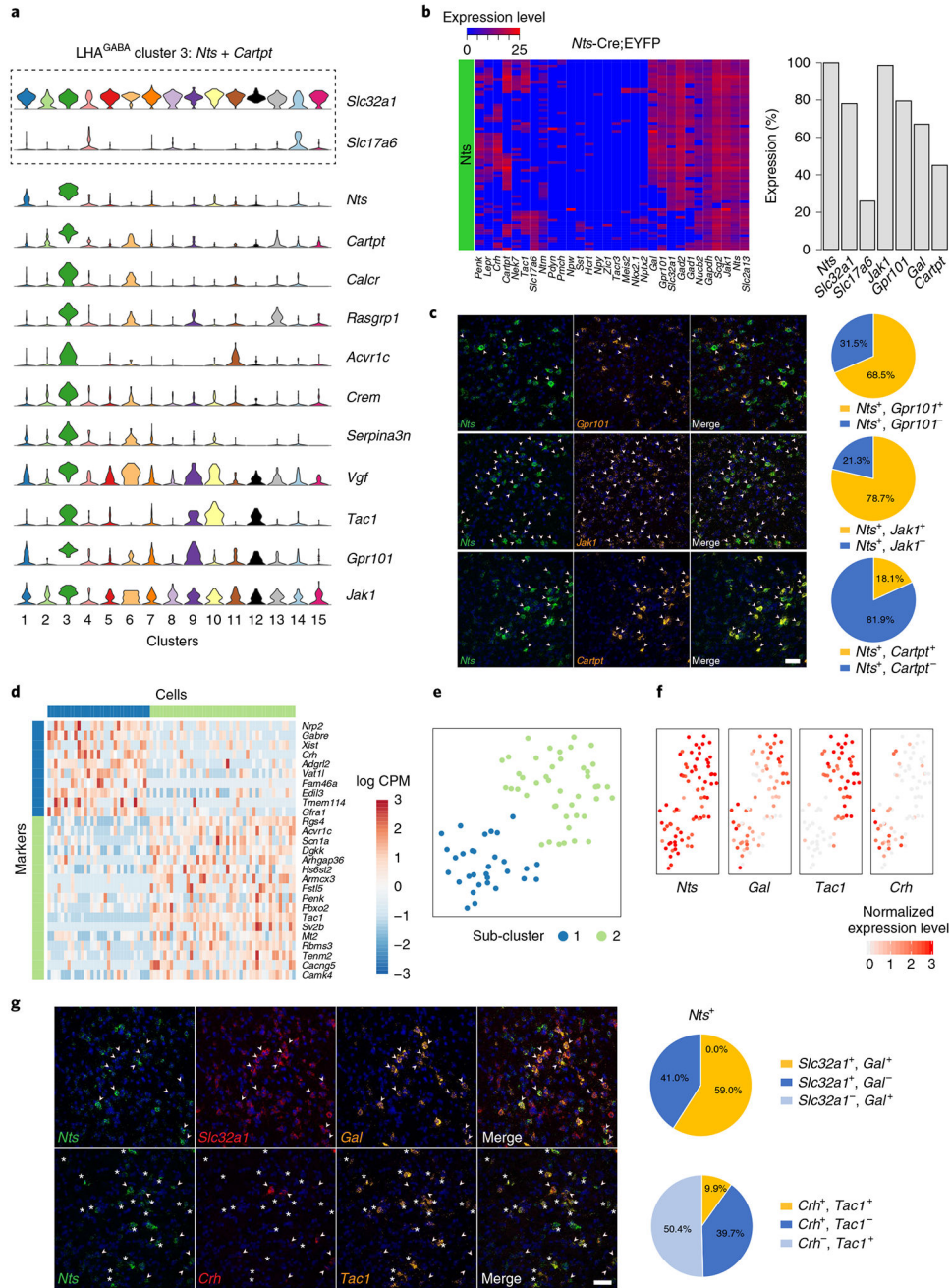
a, Violin plot, representing the distribution of log-transformed normalized gene expression (gene UMIs/total cell UMIs), of *Slc32a1*, *Slc17a6* and discriminatory markers of LHA^Glut cluster 1 (*Pmch* with *Gad1*) neurons (*n* = 119 cells). Total number of cells, mean genes per cell and mean UMIs per cell are provided in Supplementary Table 1. **b**, Left: heatmap of 19 single *Pmch*⁺ neurons and their expression of 30 genes by qPCR (*n* = 3 mice). Heatmap colors depict expression levels on a log₂ scale from low (blue) to high (red). Right: bar graph measuring percentage expression for seven genes in single *Pmch*⁺ neurons. **c**, Confocal micrographs (×40) of coronal sections of wild-type mice and corresponding pie charts representing co-expression of mRNA for *Pmch* and *Zic1* (*n* = 251 cells, 4 mice; upper), *Pmch* and *Chodl* (*n* = 206 cells, 3 mice; middle), and *Pmch* and *Otx1* (*n* = 748 cells, 3 mice;

lower). **d**, Heatmap showing scaled expression (log counts per million (CPM)) of discriminative genes across the two *Pmch*[+] subclusters. **e**, Unsupervised clustering of *Pmch*^{+} neurons of the LHA represented as a t-SNE plot ($n = 119$ cells), showing subclusters 1 (blue) and 2 (green). **f**, Normalized expression of discriminatory markers shown as t-SNE plots (*Pmch*, *Cartpt*, *Tacr3*, *Nptx1*, *Scg2* and *Nrxn3*) ($n = 119$ cells). **g**, Confocal micrographs (×40) of coronal sections of wild-type mice and corresponding pie charts representing co-expression of mRNA for *Pmch*, *Cartpt* and *Tacr3* ($n = 283$ cells, 3 mice; upper), *Pmch*, *Nptx1* and *Cartpt* ($n = 261$ cells, 3 mice; middle), and *Pmch*, *Nrxn3* and *Cartpt* ($n = 309$ cells, 3 mice; upper). For **c** and **g**, all sections were counterstained with DAPI (blue), and white arrowheads indicate co-localization. Scale bar (applicable to all micrographs), 50 μm.

Fig. 5 |. Validation of discriminatory marker expression in LHA^Glut *Trh*-expressing neurons and subpopulations.

a, Violin plot, representing the distribution of log-transformed normalized gene expression (gene UMIs/total cell UMIs), of *Slc32a1*, *Slc17a6* and discriminatory markers of LHA^Glut clusters 8 and 12 (*Trh* with *X*) neurons (*n* = 131 cells). Total number of cells, mean genes per cell and mean UMIs per cell are shown in Supplementary Table 1. **b**, Confocal micrographs (×40) of coronal sections of wild-type mice and corresponding pie charts representing co-expression of mRNA for *Trh* and *Slc17a6* (*n* = 299 cells, 3 mice; upper), *Trh* and *Otp* (*n* = 732 cells, 4 mice; middle), and *Trh* and *Onecut2* (*n* = 274 cells, 3 mice; lower). White arrowheads indicate co-localization. **c**, Heatmap showing scaled expression (log CPM) of discriminative genes across the two *Trh*^+ clusters. **d**, Unsupervised clustering of LHA *Trh*^+ neurons represented as a t-SNE plot (*n* = 131 cells), showing clusters 8 (blue) and cluster 12 (green). **e**, Normalized expression of discriminatory markers shown as t-SNE

plots (*Trh*, *Cbln2*, *Gpr101*, *Syt2* and *Cplx1*) ($n = 131$ cells). **f**, Confocal micrographs ($\times 40$) of coronal sections of wild-type mice and corresponding pie chart representing the co-expression of mRNA for *Trh*, *Syt2* and *Cbln2* ($n = 1177$ cells, 4 mice). All sections were counterstained with DAPI (blue), and white arrowheads indicate co-localization of *Trh* and *Syt2* and white asterisks indicate co-localization of *Trh* and *Cbln2*. Scale bar (applicable to all micrographs), 50 µm.

Fig. 6 |. Validation of discriminatory marker expression in LHA^{GABA} *Nts*-expressing neurons and subpopulations.

a, Violin plot, representing the distribution of log-transformed normalized gene expression (gene UMIs/total cell UMIs), of *Slc32a1*, *Slc17a6* and discriminatory markers of LHA^{GABA} cluster 3 (*Nts* with *Cartpt*) neurons (*n* = 75 cells). Total number of cells, mean genes per cell and mean UMIs per cell are shown in Supplementary Table 1. **b**, Left: heatmap of 73 single *Nts*$^+$ neurons and their expression of 30 genes by qPCR (*n* = 3 mice). Heatmap colors depict expression levels on a log$_2$ scale from low (blue) to high (red). Right: bar graph measuring percentage expression for seven genes in *Nts*$^+$ single neurons. **c**, Confocal micrographs

(×40) of coronal sections of wild-type mice and corresponding pie charts representing co-expression of mRNA for *Nts* and *Gpr101* (*n* = 553 cells, 3 mice; upper), *Nts* and *Jak1* (*n* = 361 cells, 3 mice; middle), *Nts* and *Cartpt* (*n* = 408 cells, 3 mice; lower). All sections were counterstained with DAPI (blue). White arrowheads indicate co-localization. Scale bar (applicable to all micrographs), 50 μm. **d**, Heatmap showing scaled expression (log CPM) of discriminative genes across the two *Nts* and *Cartpt* subclusters (*n* = 74 cells). **e**, Unsupervised clustering of LHA *Nts* and *Cartpt* neurons represented as a t-SNE plot (*n* = 74 cells), showing subclusters 1 (blue) and 2 (green). **f**, Normalized expression of discriminatory markers shown as t-SNE plots (*Nts*, *Gal*, *Tac1* and *Crh*) (*n* = 74 cells). **g**, Confocal micrographs (×40) of coronal sections of wild-type mice and corresponding pie charts representing co-expression of mRNA for *Nts*, *Slc32a1* and *Gal* (*n* = 308 cells, 3 mice; upper). White arrowheads indicate co-localization of *Nts*, *Slc32a1* and *Gal*. Co-expression of *Nts*, *Crh* and *Tac1* (*n* = 1,016 cells, 3 mice; lower). White arrowheads indicate co-localization of *Nts* and *Crh*, and white asterisks indicate co-localization of *Nts* and *Tac1*. All sections were counterstained with DAPI (blue). Scale bar (applicable to all micrographs), 50 μm.
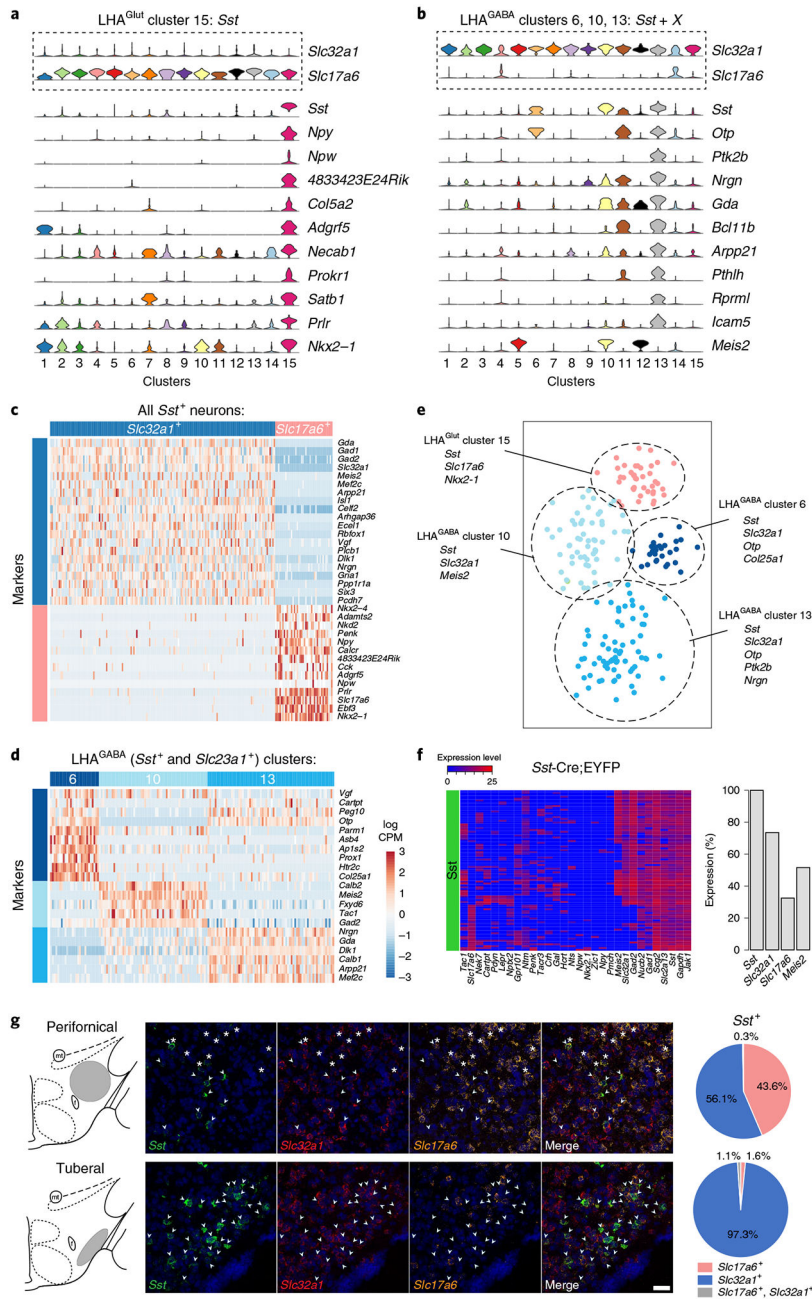
Fig. 7 |. Defining four molecularly distinct populations of *Sst*-expressing neurons in the LHA:
a, Violin plot, representing the distribution of logtransformed normalized gene expression
(gene UMIs/total cell UMIs), of *Slc32a1*, *Slc17a6* and discriminatory markers of LHA^Glut
cluster 15 (*Sst*) neurons (*n* = 40 cells). **b**, Violin plot showing normalized expression of
Slc32a1, *Slc17a6* and discriminatory markers of LHA^GABA clusters 6 (*Sst* with *Col25a*1) (*n*
= 27 cells), 10 (*Sst* with *Meis2*) (*n* = 60 cells) and 13 (*Sst* with *Otp*) (*n* = 70 cells) neurons.
Total number of cells, mean genes per cell and mean UMIs per cell are provided in
Supplementary Table 1. **c**, Heatmap showing scaled expression (log CPM) of differentially
expressed genes between *Sst*⁺ and *Slc32a1*⁺ neurons (blue) and *Sst*⁺ and *Slc17a6*⁺ neurons

(pink) ($n = 197$ cells). **d**, Heatmap showing scaled expression (log CPM) of differentially expressed genes between the three Sst^+ and $Slc32a1^+$ clusters (shades of blue) ($n = 157$ cells). **e**, Unsupervised clustering of all Sst^+ LHA neurons represented in a t-SNE plot ($n = 197$ cells). Each cell type cluster is color coded as in **c** and **d**. **f**, Left: heatmap of 87 single Sst^+ neurons and their expression of 30 genes by qPCR ($n = 3$ mice). Heatmap colors depict expression levels on a $\log_2$ scale from low (blue) to high (red). Right: bar graph measuring percentage expression for four genes in Sst^+ single neurons. **g**, Anatomical schematic of the perifornical region of the LHA (gray) (upper left). Confocal micrographs (×40) of coronal sections of wild-type mice and corresponding pie charts representing co-expression of mRNA within the perifornical LHA for Sst, $Slc32a1$ and $Slc17a6$ ($n = 952$ cells, 5 mice; upper right). Tuberal region (gray) (lower left). Confocal micrographs (×40) of coronal sections of wild-type mice and corresponding pie charts representing co-expression within the tuberal region for Sst, $Slc32a1$ and $Slc17a6$ ($n = 1,116$ cells, 5 mice; lower right). All sections were counterstained with DAPI (blue). White arrowheads indicate co-localization of Sst and $Slc32a1$, while white asterisks denote co-localization of Sst and $Slc17a6$. Scale bar (applicable to all micrographs), 50 µm.
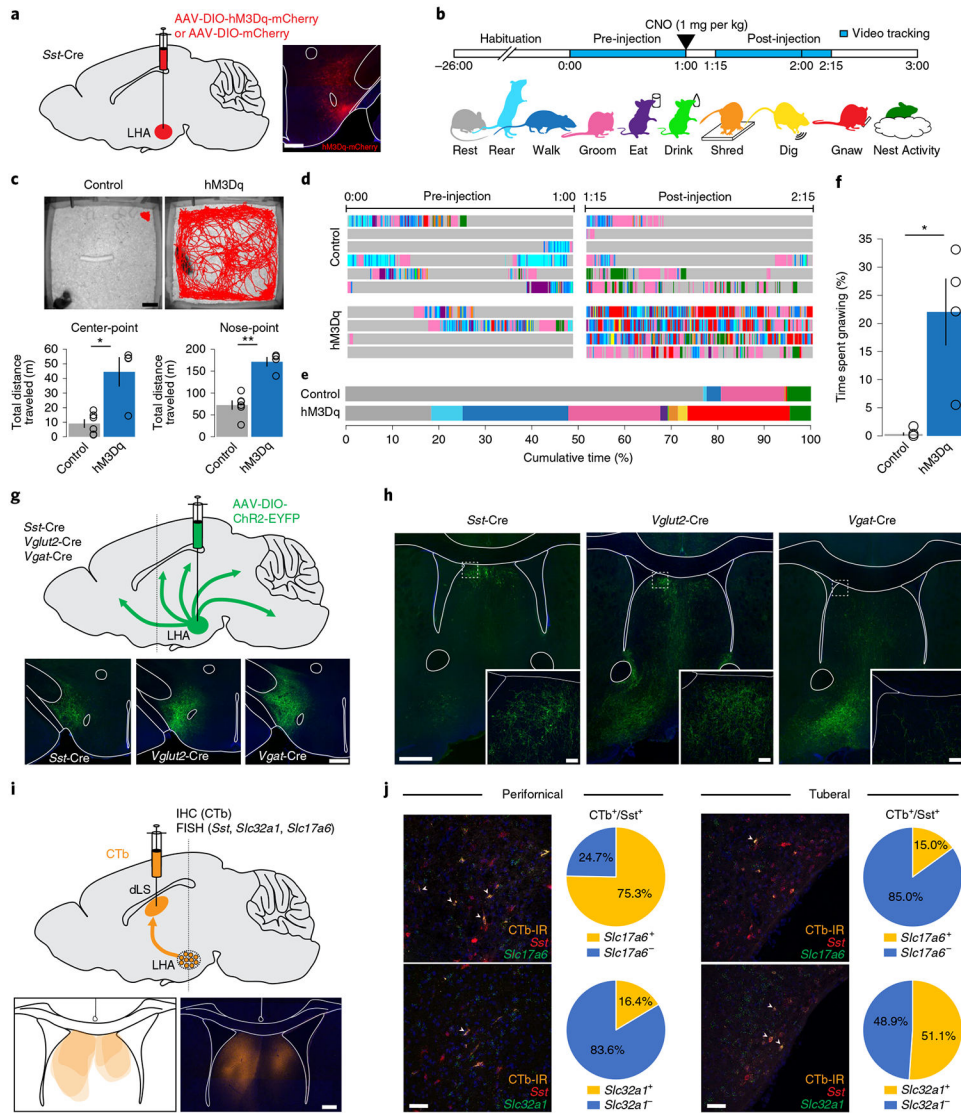
Fig. 8 |. Functional and anatomical interrogation of *Sst*-expressing neurons in the LHA:
a, Left: schematic of LHA injection site of AAV-DIO-hM3Dq-mCherry (*n* = 4 mice) or AAV-DIO-mCherry (*n* = 6 mice) in *Sst*-Cre mice. Right: fluorescence micrographs (×10) of a representative AAV-DIO-hM3Dq-mCherry injection site in the LHA of a *Sst*-Cre mouse (*n* = 4 mice). Scale bar, 500 μm. **b**, Experimental timeline (upper) and color-coded cartoon schematic representing ten murine behaviors assigned for manual scoring (lower). **c**, Upper: representative traces of mouse locomotor activity during the post-injection recording period (1 h) in a representative control mouse (left) and a hM3Dq mouse (right). Scale bar, 10 cm. Lower: bar graphs showing average distance traveled (m) in control mice (*n* = 6) and hM3Dq mice (*n* = 4), as measured using center-point (*P* = 0.038) (left) and nose-point (*P* = 0.009) (right). Open circles represent individual data points. **P* < 0.05, ***P* < 0.01 using unpaired, two-sample Wilcoxon rank-sum test. Center values indicate the mean, and error bars represent s.e.m. **d**, Color-coded behavioral heatmaps for control (upper) and hM3Dq (lower) mice during pre-injection (left) and post-injection (right) periods. **e**, Color-coded

graph of average time spent for each manually scored behavior for control and hM3Dq mice. **f**, Bar graph showing average time spent gnawing in control ($n = 6$) compared with hM3Dq ($n = 4$) mice. $P = 0.011$. Open circles represent individual data points. $*P < 0.05$ using unpaired, two-sample Wilcoxon rank-sum test. Center values indicate the mean, error bars represent s.e.m. **g**, Upper: schematic of LHA injection site of AAV-DIO-ChR2-EYFP in *Sst*-Cre ($n = 3$ mice), *Vglut2*-Cre ($n = 2$ mice) and *Vgat*-Cre ($n = 5$ mice) mice. Lower: fluorescence micrographs (×10) of representative LHA injection sites in coronal sections for *Sst*-Cre, *Vglut2*-Cre and *Vgat*-Cre mice. Scale bar, 500 μm. **h**, Fluorescence micrographs (×10) of representative LHA projection regions in coronal sections containing the dLS region (bregma +0.35 mm). Scale bar, 200 μm. Insets are corresponding ×40 confocal micrographs of LHA projections in the dLS (as indicated by the broken outline areas). Scale bar, 50 μm. **i**, Upper: schematic of dLS injection site of 0.5% CTb in wild-type mice ($n = 3$ mice). Lower: schematic representing the 0.5% CTb injection spread (orange) in the dLS ($n = 3$ mice) (left) and fluorescence micrograph (×10) of a representative injection site. Scale bar, 100 μm (right). **j**, Confocal micrographs (×40) of coronal sections of wild-type mice injected with 0.5% CTb in the dLS and corresponding pie charts representing co-expression of CTb-immunoreactivity (CTb-IR) with FISH in the perifornical region for *Sst* and *Slc17a6* ($n = 81$ cells, 3 mice; upper left), *Sst* and *Slc32a1* ($n = 67$ cells, 3 mice; lower left) and in the tuberal region for *Sst* and *Slc17a6* ($n = 40$ cells, 3 mice; upper right), and *Sst* and *Slc32a1* ($n = 45$ cells, 3 mice; lower right). All sections were counterstained with DAPI (blue). White arrowheads indicate co-localization. Scale bar (applicable to all micrographs), 50 μm.